ROBUSTNESS OF SIMPLIFIED SIMULATION MODELS FOR INDOOR MANET EVALUATION

by

Andrés Lagar Cavilla

A thesis submitted in conformity with the requirements
for the degree of Master of Science
Graduate Department of Computer Science
University of Toronto

Abstract

Robustness of Simplified Simulation Models for Indoor MANET Evaluation

Andrés Lagar Cavilla

Master of Science

Graduate Department of Computer Science

University of Toronto

2005

Evaluation of Multihop Mobile Ad Hoc Networks (MANETs) is usually performed through simulation. In these studies, it has been customarily assumed that simulation models with no obstacles are acceptable simplifications of the complex mobility and radio propagation conditions expected in actual MANET deployments.

We evaluate the robustness of simplified simulation models for indoor MANET evaluation. A simplified model is robust if the performance results it yields differ uniformly from those obtained with the unsimplified model. Robust simplifications allow researchers to reliable extrapolate simulation results to real-life situations.

We show that simplified simulation models are not robust for indoor environments. Experimentation reveals that simplifications affect two MANET routing protocols in disparate manners. Furthermore, even within a single protocol performance trends vary erratically as parameters change. These results cast doubt on the soundness of MANET evaluations using simplified simulation models, and expose an urgent need for more research in this area.

Dedication

Yo te pido capitán,

serenidad,

para mirarte

y verte crecer.

For Claudia, Beatriz and Gustavo.

Acknowledgements

This has been a great time for me. And undoubtedly, it would not have been so good without the support of my new found friends here in Canada. I want to particularly thank the guys who collaborated in this project, so much beyond what was expected: Gerard, Tom and Lionel.

I want to give a great thank you to my supervisor, Eyal de Lara. Now I know I knew next to nothing about research. Once again, thank you, for the guidance, for the steering – I know that was a big effort – and for the support.

I want to thank all my friends from Argentina who still keep in touch with me despite the distance. A big, huge hug to my grandparents, whom I miss way more than I can express.

Bust most of all I want to thank my parents: I owe you this great chance I have in life. You have made the person I am proud to be today. Los quiero.

Last but certainly not least, there is Claudia. I am so enormously happy you are walking this road with me. I will always admire and need your strength, next to me, side by side, always.

Contents

List of Tables

List of Figures

Chapter 1

Introduction

A multi-hop mobile ad hoc network (MANET) consists of a group of mobile wireless nodes that self-configure to operate without infrastructure support. MANET participants do not need access points or base stations, and instead rely on each other to establish a temporary network; peers communicate beyond their individual transmission ranges by routing packets through intermediate nodes [1, 2, 3]. Due to the mobility of the network hosts, the multi-hop routes employed for packet delivery are constantly changing. The routing protocol is therefore in charge of maintaining up-to-date routes to each network destination, both for packets originated locally and for packets generated by other nodes.

The advent of low-cost and small-sized wireless communication devices has rendered feasible the concept of MANETs and driven the intensive research in this field. However, MANET deployment is still at a very early stage [4, 5, 6]; computer simulation remains the most popular way to evaluate MANET routing protocols [7, 8, 9]. Simulation offers four important advantages:

Low cost: It enables experimentation with larger networks than those available to most research groups.

Practicality: it enables experimentation with devices and configurations that may not be feasible with existing technology; for example, mobile nodes with hybrid cellular and WiFi radio interfaces [10].

Ease of development: It allows for rapid prototyping: by abstracting the complexity of the real system, simulators enable the development and debugging of new protocols with reduced effort. This is more evident when direct execution of the actual routing protocol implementation is enabled inside the simulator [11].

Controlled analysis: It makes reproducible experiments in a controlled environment possible, facilitating the isolation of interesting conditions and the analysis of problems.

MANET protocol simulation presents challenging research problems. Besides having to simulate the networking stack and data traffic, MANET simulators also need to incorporate models of node mobility and radio propagation. The mobility model is used to simulate the behavior of network nodes, the destinations and speed they choose for their movement, and the physical paths they take. The radio propagation model is used to determine whether communication between two given nodes is possible, and to simulate the effects of interference and information loss in the wireless channel.

By definition, MANETs are suitable for hostile scenarios where no infrastructural support is available. This definition includes military operations in outdoor environments, sensor networks in environments where human intervention is not desirable or possible, and police and disaster relief operations in urban emergency situations. Recently, the application range of MANETs has extended to include other "non-hostile" scenarios such as pervasive computing settings in conference rooms or classrooms, and mesh-based wireless networks providing broadband community access. However, the preeminent models employed in MANET simulation are rather simplistic and mostly target outdoor scenarios. In the Random WayPoint (RWP) [7] mobility model, a node picks a random destination inside a flat rectangular area, proceeds to it following a straight-line trajectory at a random speed, and pauses for a fixed time on arrival. The process then repeats itself until the end of the simulation. The Free Space (FS) propagation model assumes an obstacle-free vacuum where signal strength degrades with the square of the distance between the transmitter and receiver.

Both of the aforementioned models assume scenarios devoid of obstacles. Although this might be a reasonable assumption in certain outdoor situations, it is likely not applicable in many environments where the impact of a larger number of obstacles on both node mobility and radio propagation cannot be underestimated. Although several groups have extended these simple obstacle-free models with increasing levels of detail [11, 12, 13, 14, 15, 16], the majority of the research on MANET simulation models has still focused on outdoor environments. Indoor environments are well known to present different challenges, due to the concentration of a variety of structures and construction materials in a much reduced area. Moreover, most of the research on MANET simulation models has focused on quantifying the differences in routing protocol performance introduced by an arguably better model, but has not attempted a higher level characterization of the properties of simulation models.

This thesis evaluates the *robustness* of simplified mobility and radio propagation simulation models for MANET simulations in indoor environments. A simplified simulation model is *robust* if the results obtained with the model for different routing protocols and simulation conditions are consistent (within a predictable error) with the results yielded by the unsimplified model. A robust simplification allows researchers to extrapolate simulation results over different scenarios, and reach reliable conclusions about the expected performance of protocols in real life. Therefore, robustness (or its lack of) in a simplified simulation model is a qualitative indicator of the applicability of the model, and the relevance of the results obtained through its use.

To determine the robustness of simplified models for indoor MANET simulation, we first introduce two detailed simulation models – one for mobility and one for radio propagation – that take into account fine-grained obstacles and building materials. We then describe several simplifications to these detailed models that gradually decrease in sophistication. The least detailed models we consider correspond to the obstacle-free approaches provided in most MANET simulators (i.e., RWP and FS).

Experiments with DSDV [2] and DSR [1], two representative MANET routing protocols, show that simplifications to the mobility and radio propagation models are *not robust*, and have instead drastically different effects on the perceived performance of the two routing protocols. Whereas the performance of DSDV is virtually identical for all models, the performance of DSR varies widely between models. Moreover, even within DSR itself, the relative performance under the different models changes erratically as we vary experimental parameters. These findings raise troubling doubts over the soundness of MANET protocol evaluations based on simplified models, and expose the urgent need for more research on realistic MANET simulation models for indoor environments.

This thesis makes thus two contributions: first, it shows that widely used simplified mobility and radio propagation models are not robust. We provide experimental evidence showing that the effects of simplifications of the simulation model are not uniform across protocols and evaluation conditions, hence leading to wrong conclusions about the performance of MANET protocols. Second, it provides the first evaluation of MANET routing protocols in indoor environments using detailed mobility and radio propagation models that account for fine-grained obstacles and building materials.

The rest of the thesis is organized as follows. Chapter 2 describes the usual techniques and models in MANET simulation, and reviews wireless MAC and MANET routing protocols, with an emphasis on 802.11 DCF, DSR and DSDV, the protocols employed in our simulation study. Chapter 3 describes the main characteristics of indoor environments, and the challenges such characteristics present for MANET simulation. Chapters 4 and 5 present our detailed mobility and radio propagation models for indoor environments, describe simplifications to each model, and report how the models were implemented inside the ns2 network simulator. Chapter 6 presents our experimental results. Finally, chapter 7 compares the thesis to previous work on sophisticated mobility and radio propagation models, and chapter 8 presents our conclusions and discusses avenues for future research.

Chapter 2

Background

During the mid 1990's, researchers in MANET routing protocols would each independently build their own wireless networking simulator. The disadvantage of lacking a uniform and commonly agreed-upon evaluation tool, and the fact that simulator validation for each different system was mostly missing, constituted clear drawbacks in this approach. The first complete simulation framework for performance evaluation of MANET routing protocols was presented by the CMU monarch project in [7]. This seminal paper had three main contributions:

- Several pieces of software were built for the *ns2* network simulator [17] – usually employed in the analysis of wired networks – to enable wireless ad-hoc networking simulation. These enhancements are usually referred to as the CMU Monarch ns2 Wireless Extensions [18]. Among other things, the simulator was augmented with an implementation of the IEEE 802.11 Distributed Coordination Function (DCF) MAC protocol, implementations of several routing protocols, tools to generate node mobility patterns, and the capability to simulate a wireless shared channel with different propagation and modulation models.

- A methodology for the performance comparison of several routing protocols was presented. The base mobility and radio propagation models employed, as well as the simulation parameters chosen, were later reused by a number of researchers in all types of

MANET simulation studies.

- The results of the performance study showed the first bits of insight into the requirements and pitfalls of good routing protocol design.

Building on the contributions of the Monarch work, a spate of MANET simulation studies were produced [8, 9, 19, 20, 21, 22, 23, 24], backed up by the MANET research community's reliance on this framework. Moreover, other MANET simulation tools such as GlomoSim [25] and OpNet Modeler [26], have also been adopted alongside ns2.

In the rest of this chapter we will provide a brief overview of the internals of the ns2 network simulator. We will then describe the mobility and propagation models implanted by the Monarch group for MANET simulation. Finally, we will review the MAC and routing protocols usually employed in MANET research, as well as in this thesis: the IEEE 802.11 DCF, DSR, and DSDV.

2.1 The ns2 Network Simulator

Th ns2 Network Simulator [17] is an open-source object-oriented discrete-event simulator for network research. The simulator is written in C++, with an OTcl (Object Tool Command Language) interpreter used as the command interface. The C++ part constitutes the core of the simulator, where detailed protocol implementation and the simulation engine are located. The OTcl part, on the other hand, is used for simulation configuration. Therefore, the only prerequisite to use the simulator is a basic knowledge of OTcl, needed to specify the objects involved in the simulation scenario and the values of the various objects' parameters. However, to develop new models and protocols, the C++ core and its bindings to the OTcl external interface need to be thoroughly understood. The learning curve for the intensive user of the simulator is therefore quite steep.

One of the main advantages of the split-language implementation of ns2 is its object oriented design, which allows for easy replacement of the software modules involved in a simu-

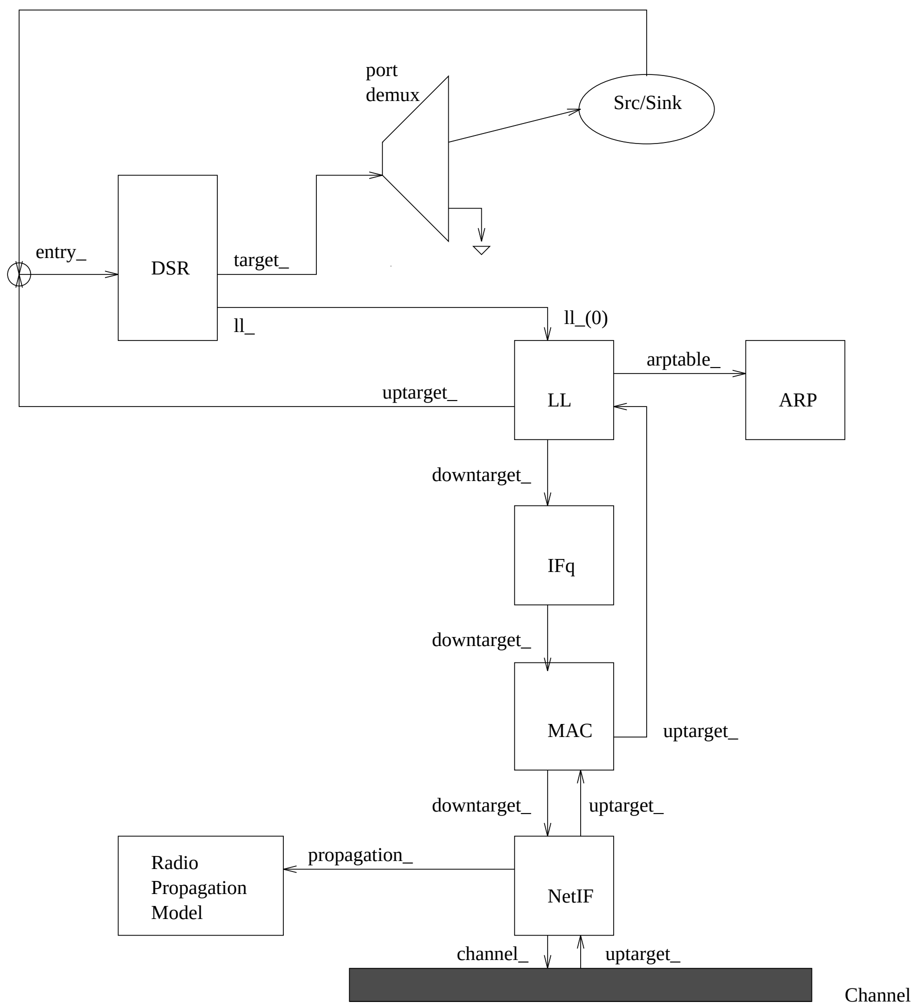

Figure 2.1: Typical MANET node configuration in ns2.

lation — for example a routing protocol, a network application, or a propagation model. The process of configuring the set of modules required to perform a particular simulation, starting from the physical interface model up to the application layer, is known as *plumbing*, and is usually performed by an OTcl script. A developer testing a new protocol, or implementing a simulation model, needs to write the code with the correct bindings to the OTcl interface, and afterwards instruct the plumbing script to employ the newly created modules during simulation setup.

Figure 2.1 illustrates the plumbing for the network stack objects of a MANET node that uses the DSR routing protocol: an application layer module, the routing protocol, the Address Resolution Protocol (ARP) module, a Link Layer object, an interface queue, the MAC protocol, and the physical interface with the channel's radio propagation model.

2.2 The Random Waypoint Mobility Model

The preeminent mobility model used for MANET simulation is the Random WayPoint (RWP) model, introduced by the Monarch group [7]. RWP assumes that node mobility takes place in a flat rectangular area with no obstacles. Node movement is characterized by two parameters: a speed interval $[V_{min}, V_{max}]$ and a pause time P. The movement pattern of mobile nodes follows a cyclic behavior: a node pauses for P seconds, chooses a random destination inside the simulation rectangle, and randomly selects a speed within the speed interval. The node then moves toward its new destination at the chosen speed, following a straight-line trajectory and unhindered by any obstacles or the presence of other nodes. Upon the node's arrival to its destination, the process resumes.

RWP represents a generic approach to node mobility, and consequently it also is a very simplistic model. The shortcomings of RWP can be categorized under two different aspects:

Behavioral modeling: nodes move in a completely random manner, without following any purpose or trying to complete any task. From a logical point of view, a node can choose destinations from an infinite set. Moreover, past behavior of a node does not affect future decisions.

Physical Modeling: nodes move in an idealized flat scenario where there are no obstacles; there is no need to open a door, avoid a pit or climb a hill. Furthermore, two nodes can occupy the same physical location simultaneously.

Given its widespread use within the MANET research community, the RWP model and its properties have been the subject of extensive research [27, 28]. We draw attention here to two interesting characteristics:

Density waves: A *density wave* is the clustering of nodes in one part of the simulation area. RWP tends to periodically accumulate nodes in the center of the simulation rectangle. This happens because whenever a node chooses a location near the boundaries of the simulation area, with high probability its next destination will make it travel through the center of the simulated rectangle.

Average Speed Decay Effect: As simulation time progresses, the average speed of the nodes in the simulation tends to decrease significantly. This happens because an increasing number of nodes are moving toward distant locations at a very low speed [27]. The most straightforward way to solve this problem is to specify a non-zero V_{min} value, such as 0.5 m/s.

Despite being widely used, the deficiencies of RWP are also well documented. It is therefore not surprising that several researchers have proposed alternative mobility models targeting the behavioral or physical modeling simplifications of RWP. We will describe such related work in section 7.1.

2.3 The Free Space Radio Propagation Model

The preeminent radio propagation model in MANET simulation is the Free Space (FS) propagation model. In the same vein as RWP, FS assumes a flat space devoid of obstacles. Radio wave power degradation is thus proportional to the square of the distance between transmitter and receiver, exclusively. The FS model is described by Equation 2.1 (in Watts) and Equation 2.2 (in dBm)

$$P_{FS}(r) = \frac{P_t G_t G_r \lambda^2}{(4\pi)^2 r^2 L} \tag{2.1}$$

$$P_{FS}(r) = P_o(r_0) - 20\log_{10}\left(\frac{r}{r_o}\right), \tag{2.2}$$

where r is the distance between transmitter and receiver, P_t is the transmitted signal power, G_t and G_r are the antenna gains of the transmitter and receiver, respectively, λ is the wavelength (speed of light over frequency), and L $(L \geq 1)$ is the system loss due to miscellaneous sources. It is common to select isotropic (or unity gain) antennas, $G_t = G_r = 1$, and no system loss, $L = 1$. In Equation 2.2 P_o is the power in dBm at a reference distance r_0, which is nominally set to 1 meter; the conversion rule between dBm and Watts is $P_{dBm} = 10\log_{10}(P_{Watts} * 10^3)$.

FS propagation has been widely adopted because it is computationally inexpensive: signal strength can be computed only with a few floating point operations. Moreover, given that FS is a one-to-one relation between power and distance, it can be easily characterized in terms of the *sensitivity threshold* employed, i.e. the cutoff power value that determines the minimum signal strength needed for a node's wireless interface to understand an incoming transmission. After placing the sensitivity threshold value on the left hand side of Equation 2.1 or 2.2, solving for the r distance value will yield the radius of the coverage disc of a node, the circular area inside which connectivity to other nodes can be established. We call this distance value the *effective communication range*; it is a quantity widely used to characterize the degree of connectivity in a network using FS propagation.

For large environments with distances greater than a hundred meters, the Two-Ray Ground propagation model is favored over FS. This model considers the aggregate effects of radio waves converging by two different paths on the receiver: the direct line-of-sight path, and a second path reflecting off the ground. The Two-Ray Ground model is given in Watts by

$$P_{TRG}(r) = \frac{P_t G_t G_r h_t^2 h_r^2}{r^4 L}, \tag{2.3}$$

where h_t and h_r are the antenna heights at the transmitter and receiver, respectively, and are usually set to $h_t = h_r = 1.5$ m; the remaining parameters hold the same meanings as in FS. Two-Ray Ground has been shown to yield better accuracy than FS for long distances [29].

A hybrid propagation model, combining both FS and Two-Ray Ground, has been implemented in ns2 by the Monarch group: a cross-over distance is determined by $d_c = (4\pi h_t h_r)/\lambda$, which represents the distance at which both models result in the same signal strength. For distances $r < d_c$, FS is employed; for distances $r > d_c$, Two-Ray Ground is employed. For radio wave frequencies of 900 MHz and 2.4 GHz, the threshold distance d_c is equal to 86.14 m and 227.33 m, respectively. Given that in this thesis we analyze radio wave propagation in indoor environments at 2.4 GHz, we will employ exclusively Free Space propagation.

Because the FS and TRG models neglect the presence of obstacles, they do not account for multipath fading effects: the different ways in which radio waves interact with obstructions in their trajectories. The multipath effects are categorized as follows:

Reflection occurs when a radio wave impinges upon an object which has very large dimensions compared to the wavelength of the propagating wave.

Diffraction occurs when the radio path between the transmitter and receiver is obstructed by a surface that has sharp irregularities (edges). The secondary waves resulting from the obstructing surface are present throughout the space and even behind the obstacle, giving rise to a bending of waves around the obstacle, even when a line-of-sight path does not exist between transmitter and receiver.

Scattering occurs when the medium through which the wave travels consists of objects with dimensions that are small compared to the wavelength. Several radio waves are radiated from the relatively small obstacle in different directions

Beyond disregarding the various multipath fading effects, the FS model has other disadvantages:

Idealized Transceivers: FS assumes isotropic (unity gain, or 0 dBi) and omni-directional antennas. The former is not problematic, since the effects of antenna gains different than unity can be factored in the model, as we will show later. The assumption of an omni-directional antenna is, on the other hand, quite unrealistic and troublesome: RF transceivers are not necessarily omni-directional, and even those that are suffer changes in their radiation pattern by the significant obstruction that represents the body of the carrier. This has been shown quite conclusively in [30], where special provisions had to be taken to account for the orientation of the RF interface.

A Time-invariant Channel: whereas FS attempts to model large scale fading – the degradation of signal strength in large areas assuming a static environment –, it does not consider the effects caused by small scale fading, those attenuations on signal strength caused by small changes in the environment, as small as half wavelength [31]. These small changes alter the delay in each path of a multipath system differently, thus causing dramatically large variations in signal phase and signal strength, usually in the order of 20 to 30 dB. In mobile radio communication systems, the effects of small scale fading manifest themselves as a time-variant channel. For many propagation models employed in MANET, including FS, the channel is assumed to be time-invariant or static, and the effects of small-scale fading are ignored.

Two-Dimensional environment: FS assumes a flat area; Two-Ray Ground provides basic consideration for different heights in the transmitter and receiver antennas.

An important number of research publications present alternatives to the FS model for MANET simulation. We will review these proposals in section 7.2.

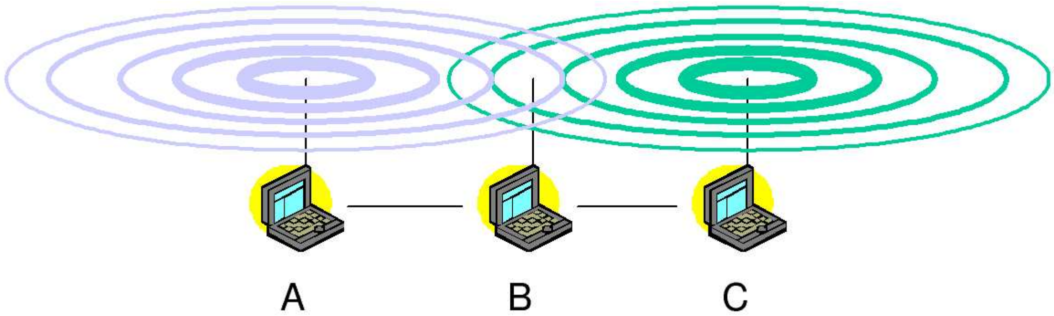

Figure 2.2: The Hidden Terminal problem in wireless networks.

2.4 Wireless MAC protocols

A crucial part of a wireless communication system is the Medium Access Control (MAC) protocol. Broadly speaking, the MAC protocol arbitrates use of the communications channel. A significant problem that arises in wireless networks is the *hidden terminal* problem, illustrated in figure 2.2. Consider the scenario where computer C attempts to send a packet to computer B, and simultaneously A also attempts to communicate with B. A and C cannot detect each other, given the distance separating them; however, both transmissions collide in the vicinity of B, causing a jam in the channel. A and C are acting as *hidden terminals* with respect to each other.

Several MAC protocols have been proposed, with increasing degrees of overhead and better handling of the hidden terminal problem: Carrier Sense Multiple Access (CSMA) [32], Multiple Access with Collision Avoidance (MACA) [33], Floor Acquisition Multiple Access (FAMA) [34], and the IEEE 802.11 Distributed Coordination Function (DCF) [35]. The 802.11 DCF MAC protocol is a CSMA/CA protocol (carrier sensing with multiple access/collision avoidance); it is also the most popular choice for MANET systems deployment and simulation. Furthermore, the IEEE 802.11 technology can be identified as one of the main reasons behind the widespread growth of wireless networking: the industry alliance backing up its development is known as WiFi.

In 802.11 DCF, competing nodes that wish to transmit a packet wait for a random period of time before attempting to acquire the channel. Once the random wait period has expired, a transmitting host will sense the channel, expecting it is not currently in use; this operation is called *carrier sensing*. There are two types of carrier sensing: physical carrier-sensing, an operation dependent on the underlying physical interface, and virtual carrier sensing, the checking of the Network Allocation Vector (NAV), a timer set by the currently transmitting node indicating when it expects to be finished. Usually, a node first checks its NAV, and if it indicates that the channel should not be in use, then it performs physical carrier sensing. Note that the host with smallest random wait period will sense the channel before its neighbors and thus gain access.

If the carrier sense operation has been successful and the host knows the channel is not in use, a Request-To-Send (RTS) control packet announcing the incoming transmission is broadcasted, with a NAV value equivalent to the expected channel occupancy period. Upon reception of the RTS, the destination node replies with a Clear-To-Send (CTS) control packet. Every host receiving any of the RTS or CTS announcements knows that somebody in the vicinity will be using the shared channel to receive a packet transmission, and it also knows for how long; the hidden terminal problem is thus avoided.

If either the carrier sense fails, because the wireless channel is occupied, or there is a timeout while waiting for the CTS response, the node waits for a random backoff period (after the expiry of the current NAV) before attempting a new carrier sense and CTS/RTS exchange. The usual 802.11 implementation allows seven retries of this operation before dropping the packet; the backoff period window grows exponentially for each new retry.

After the RTS originator receives the CTS answer from the destination of the packet, it proceeds to broadcast the DATA packet. If the transmission of the DATA packet is successful, the receiving node will send a positive acknowledge (ACK) packet, thus finishing the transmission process. The usage of ACK packets serves two purposes. It enables the retransmission of packets upon failure, and it lessens the impact of the hidden terminal problem with mobile nodes. In a mobile node scenario, a host might be able to interfere with a packet transmission by moving within the connectivity region of the communicating terminals, after the RTS-CTS exchange has taken place. ACK packets allow swift detection of this problem.

The RTS/CTS exchange is not always used in 802.11 DCF. A threshold on packet size is placed to determine which packets need this operation; smaller packets are sent using only carrier sensing. Control packet exchanges are also avoided for the transmission of broadcast packets, aimed to every node within connectivity reach.

While 802.11 is usually employed as the MAC protocol in MANET research, there has been some work regarding the interactions of different routing and MAC layer protocols [36,37]. It is worth pointing out that the performance of MANET routing protocols is greatly influenced by the behavior of the underlying MAC protocol: for example, extensive use of unicast messages in 802.11 might degrade the performance of the network, as the channel is occupied with many RTS/CTS/DATA/ACK control exchanges [9, 21].

2.5 MANET Routing Protocols

MANET routing protocols fall into two broad categories: reactive and proactive. Reactive routing protocols, also known as on-demand, only create or update routes when packets need to be transmitted along them. A route discovery process is initiated, flooding the network with a query to find the desired route, which is cooperatively constructed by the replies of each node in the network. On the other hand, proactive routing protocols try to keep up-to-date routing tables at all times. Nodes keep routing tables with entries for each destination, and react to changes in the network by propagating the modifications to their tables in order to obtain a consistent network view. This is the typical behavior of wired-network routing protocols such as OSPF, broadly used in the Internet.

Among the reactive proposals, DSR [1, 38] and AODV [3] are the most well known. Experimental RFCs of both of these protocols have been proposed in the IETF MANET workgroup [39], and implementations for UNIX-based operating systems are currently available [18, 40]. Other on-demand routing protocol proposals include the Temporally Ordered Routing Algorithm (TORA) [41] and Associativity Based Routing (ABR) [42].

Destination-Sequenced Distance Vector (DSDV) [2] is the most salient proactive routing protocol, and arguably the first ad hoc routing protocol. The Wireless Routing Protocol (WRP) [43] is another early ad-hoc routing protocol. The Clusterhead Gateway Switch Routing (CGSR) [44] protocol is a hierarchical protocol that divides the network into clusters; a particular node called the clusterhead centralizes communication to destinations outside each cluster. CGSR uses DSDV for both intra and inter cluster routing. Another hierarchical proactive routing proposal is the Optimized Link State Routing Protocol (OLSR) [45], which has gained great acceptance among the members of the IETF MANET charter.

There are also routing protocols which do no fit the binary categorization we have used. For example, the Zone Routing Protocol (ZRP) [46] is a hierarchical and hybrid proposal, where a proactive component is used inside the local region, and a reactive component is used for inter-region routing. Location-aided routing protocols that use GPS or other means or geographical absolute localization, such as Location-aided Routing (LAR) [47], Distance Routing Effect Algorithm for Mobility (DREAM) [48], and the Geographical Routing Algorithm (GRA) [49], are also quite popular.

We next describe the two routing protocols we have used in this thesis: DSR (on-demand) and DSDV (proactive). For a more thorough review of MANET routing alternatives, the interested reader can refer to [50]; a synthesis of the (relatively) current state of affairs in the IETF MANET charter can be found at [51].

2.5.1 DSR

DSR is a proactive routing protocol, in which routes are discovered on-demand. The key feature of DSR is the use of *source routing*: the sender computes the route through which a packet will be forwarded to its destination. Each packet thus carries in its header the full route to its destination, and the the task of intermediate nodes is to forward the packet to the next hop in the attached source route.

Each DSR node keeps a *route cache*, filled with routes the node discovers on demand, or that it overhears from packets placed in the channel. DSR nodes operate their radio interfaces in promiscuous mode, listening to every packet transmitted in the shared channel, and thus can take advantage of the source routes present in each packet's header. If the local node is detected in the overheard source route, the segment of the route involving the local node, up to the intended destination, is stored in the route cache for potential future use. Naturally, a DSR node will also place in its cache interesting route segments that it might extract from packets it is forwarding.

When a packet needs a route, DSR first tries to retrieve a suitable entry from its cache. If successful, the route is applied to the packet's header and the packet is dispatched to the first hop in the route. Otherwise, DSR switches to *route discovery* mode, and sends a *route request* broadcast message with an empty source route. Upon receipt of a route request, a node attempts to answer it with a suitable cached route; it generates a *route reply* message with the cached route appended to the route found in the route request message – processed to remove loops –, and unicasts the reply back to the request originator using the route currently present in the request, but reversed. To prevent collisions in the channel from neighboring answering nodes, the route reply messages are randomly jittered. Moreover, if a route reply is overheard during the jittering time, targeted to the same requester and with a shorter or equal route length, the route reply packet is silently dropped. If no suitable route is found in the cache, the node appends itself to the source route of the route request message and rebroadcasts it.

To prevent the formation of loops, a node checks that its own address is not already present in the source route of the route request message it has received; otherwise it discards it. Moreover, to prevent duplicate answering, route request messages are tagged with a monotonically increasing sequence number generated by the requester. A node keeps track of the route requests' sequence numbers it has recently served, and is thus able to identify route discoveries on which it has already collaborated. To further enhance the route discovery process, the originating node first broadcasts a *non-propagating route request* (or zero-ring search), a route request that cannot be forwarded by other nodes. In this way, the requester can inexpensively check if the target of the route request is within its current set of neighbors, and it can also learn routes without propagating the request to the whole network. If the non-propagating request fails, then an unrestricted route request message is broadcasted.

As nodes rebroadcast a route request, the message will eventually reach the target destination. The target node will then construct a a unicast *route reply*, by reversing the route found in the route request. Since the route request will propagate through many different paths, the route discovery process can therefore generate many different route replies with different routes. Notice that if after a timeout period the originator of a route request receives no answers, it will exponentially backoff and try again. Eventually, the requester will give up, cease asking for routes and drop the packet.

Apart from route discovery, the standard operating mode of a DSR node is *route maintenance*. During route maintenance, DSR nodes forwards packets, overhear source routes and cache them, and participate in route discovery process. DSR nodes can also send gratuitous route replies; if a node overhears a packet that will eventually reach it, but whose source route contains a segment between the current transmitter and the overhearing node longer than one hop, the node will then alert the originator of the packet – not necessarily the current transmitter – that the route can be shortened, using a route reply that will be hopefully overheard and thus cached by many other nodes.

Whenever a packet fails to be sent to its next hop by the MAC layer, DSR assumes the link is broken. DSR then cleanses its cache of every route using the apparently broken link, and sends a unicast *route error* message to the originator of the packet. Every node that overhears a route error message, including the final destination of the packet, will also remove routes using the link from its route cache. Upon receiving the route error packet, the sender attempts to find a new route to the destination node in its route cache, and if none is found, switches to the route discovery mode.

Non-propagating route request (RREQ) timeout	30 ms
Time between non-propagating RREQs, for different destinations	5 sec
Time between retransmitted non-propagating RREQs	500 ms (exponentially backed off)
Maximum route request timeout	10 sec
Maximum rate for sending replies to a route	1/sec
Maximum number of unsolicited replies being held off	10
Time to hold packets awaiting routes	30 sec
Packet buffer size	64
Route error holdoff time	1 sec
Size of source route header with n addresses	$4n+4$ bytes
Maximum number of times a packet can be salvaged	15
Number of flow initiator packets needed	3
Flow table entry timeout	60 sec

Table 2.1: DSR protocol constants.

DSR is further optimized through two techniques, *packet salvaging* [38] and *implicit source routing* [52]. When an intermediate node fails to forward a packet through a link, the traditional behavior of DSR is to remove from the node's cache the routes involving the failing link, and afterwards send the appropriate route error message. With packet salvaging, the node also attempts to salvage every packet currently present in its queue of pending transmissions that were to be sent through the failing link. DSR will use the route cache to replace the source route of such packets with cached alternatives. The packets are then reinserted at the back of the queue. To prevent infinite salvaging, there is a threshold placed on the maximum number of times this optimization can be applied to a packet.

Implicit source routing is an optimization targeted to minimize the byte overhead of tagging every packet header with a source route. Each node in the network keeps a *flow table*. When the originator of a packet wishes to establish an implicit route, it sends a number of *flow initiator* packets, traditional packets with their source route, the appropriate flag and a *flow identifier*. Each hop in the route will create an entry in its flow table for this flow identifier with the associated route. Every packet forwarded through that route from now on does not need to carry the full source route in its header, but rather only the flow identifier. Flow table entries timeout if not used recently, and unicast *flow unknown* error messages are sent back to the transmitters of packets with unknown flow identifiers. Upon reception of a flow unknown message, the node will contact the source of the implicit route and instruct it to reestablish the flow.

Table 2.1 lists the DSR constants employed in the protocol's implementation contained within the ns2 simulator version 2.26.

2.5.2 DSDV

DSDV is a table-driven proactive routing protocol, that builds on the Bellman-Ford distance-vector routing algorithm [53]. In DSDV, every node has a routing table, with one entry per destination node in the network. Besides the destination's address, each routing entry includes the next hop to the destination, a metric (usually the path length), and the sequence number of the first hop in the route, to indicate the freshness of the information. A DSDV node thus only knows the first hop in the route through which it will forward a packet to its destination. Application layer packets are tagged with the destination address, and every intermediate hop needs to check its corresponding routing entry to find out where to forward the packet next.

DSDV is called a proactive protocol because nodes actively exchange routing information, regardless of the need for it, and constantly maintain routes for every possible source-destination pair in the network. This fixed overhead might be unnecessary in environments with lower routing requirements.

DSDV routing information is only exchanged through broadcast advertisements. In each advertisement, a node publishes a monotonically increasing even sequence number for itself, and the contents of its routing table. By exchanging this information, nodes can reach a consistent view of the network. A node analyzes the information contained in the advertisements, and determines if a route to a given destination through the advertising node will have a smaller metric than the route actually in use – or the same metric but with a fresher sequence number –, and thus modifies its own routing table accordingly.

There are two types of advertisements: periodic and triggered. Periodic updates are full updates, scheduled at regular times, in which the whole local routing table is advertised to the neighboring nodes. Triggered updates are on the other hand incremental updates; they are caused by topology changes detected by a node which need immediate propagation to the rest of the network. Therefore, only the routing information that changed since the last advertisement needs to be propagated. However, if the incremental routing information to be transmitted surpasses a certain threshold, then the incremental update will be upgraded to a full-scale periodic update. As a side-effect, the actual scheduling for the next periodic advertisement is also modified.

DSDV decides a link is broken after a number of expected periodic updates have not been received. In this case, the DSDV node will advertise an infinite metric and an odd sequence number for that node, equal to the last known sequence number plus one. This ensures that whenever the node on the other side of the suspect broken link becomes connected again, the sequence number it will advertise will overwrite all the information about the broken link. Another interesting effect of the use of monotonically increasing sequence numbers in DSDV is that loop-freedom is guaranteed in the formation of routes.

The DSDV standard is unclear as to whether triggered updates should be sent when a new route metric is found, or when a new sequence number is found. Sending updates on new sequence numbers will result in a higher responsiveness in the network when broken links are detected, at the cost of exchanging sometimes unnecessary information that will not enhance the routing task. The propagation of triggered updates is further subjected to a set of timing constraints: a weighted settling time specifies the time a node waits between reception of a triggered update and broadcasting its own resulting triggered update; an aggregation time is further specified such that no two updates by the same node can be transmitted in less than such time. The objective of these constraints is to avoid “broadcast storms”, i.e. the triggering

Periodic route update interval	15 sec
Periodic updates missed before link declared broken	3
Route advertisement aggregation time	1 sec
Maximum number of packets buffered per node per destination	5
Initial triggered update weighted settling time	6 sec
Weighted settling time weighting factor	7/8
Updates triggered on receipt of a new sequence number	No
Updates triggered on receipt of a new metric	Yes
Threshold for upgrading triggered updates to full updates	1/3 of table size

Table 2.2: DSDV protocol constants.

of broadcasts for every node of the network in a chain reaction.

Table 2.2 lists the DSDV protocol constants employed in the DSDV implementation contained within the ns2 simulator, version 2.26.

Chapter 3

Indoor MANET Simulation

The use of MANETs in indoor environments has been envisioned for many interesting applications. We list a few of these cases:

- Disaster relief teams, such as firemen.
- Police operations.
- Pervasive computing environments.
- Conferences or classrooms.

MANET simulation in indoor environments presents interesting challenges. Modern buildings usually have irregular shapes and large numbers of obstacles, which affect both node mobility and radio propagation. Moreover, indoor environments tend to be much smaller than the outdoor scenarios traditionally considered in MANET research, amplifying the influence of the obstacles on the network's behavior. Finally, buildings typically have multiple floors, which adds a three-dimensional aspect to the simulation.

For instance, consider Figure 3.1, which shows the blueprint of the fifth floor of the Bahen Centre for Information Technology, an academic research building located in the St. George Campus of the University of Toronto. The building stands on a 113 by 88 meters lot, and the area of the depicted floor plan is the same as that of a square with 73.5 meter sides. This

Figure 3.1: Blueprint of the fifth floor of the Bahen Centre for Information Technology.

area is a hundred times smaller than what is usually considered in MANET simulations: for example, [7, 9] perform MANET simulations in a rectangle of 300 by 1500 meters. The figure also portrays the irregular layout of this building, but barely conveys a sense of its architectural complexity: cement pillars, steel shafts, brick walls, and the pervasive presence of glass are just some of its relevant characteristics. Also, elevators and stairs can be used to move between the multiple floors of the building. Finally, given that the environment under consideration is not the ground floor, movement outside the floor plan is – for all practical purposes – impossible.

In the following chapters, we describe detailed node mobility and radio propagation models that address the challenges presented by indoor environments such as the one aforementioned. In order to assess the impact of modeling different incremental features, for each model we present several simplifications; we gradually remove levels of detail in the models until we fall back into the obstacle-free models described in chapter 2. The interested reader will find a comprehensibly documented and freely-available distribution of the ns2 implementations of these models in www.cs.toronto.edu/~andreslc/papers/MANET_extensions.tgz. Notice that these models are currently targeted to simulations of a single floor; extending the models to support multiple-floor simulation is left as a future research objective. Finally, in chapter 6 we present the most important contribution of this thesis, the evaluation of the robustness of these simplifications for indoor environments.

Chapter 4

Constrained Mobility Model

We introduce Constrained Mobility (CM), a novel mobility model for simulation of complex indoor environments. CM uses a *mobility graph* to constrain node mobility according to the obstacles present in the environment. For instance, a mobility graph has been drawn over the blueprint of the Bahen's fifth floor, as illustrated in Figure 4.1. Vertices represent possible destinations that nodes can visit, and edges correspond to physically-valid paths over which nodes can move toward their intended destinations. Movement from one destination to another is accomplished by traversing the edges that constitute the shortest path between the two corresponding vertices. Therefore, nodes move through doors and hallways to reach their destinations, instead of resorting to straight-line trajectories.

At present, we draw the mobility graph on top of the floor plan using a simple graphical editor we developed — a screen capture of the editor is displayed in Figure 4.2. CM graphs are drawn using existing AutoCAD drawings. This is not a laborious task, and is furthermore completely amortized by the large number of times the graph for a given floor plan is used in different simulations. For example, the graph used throughout this thesis was first drawn in 30 minutes, and later subjected to minor refinements that were also applied in a matter of minutes. Nevertheless, we plan to explore techniques to automate the generation of mobility graphs, by using the publicly available AutoCAD [54] format to parse the blueprint of interest.

(a) Blueprint of the fifth floor of the Bahen Centre for Information Technology.

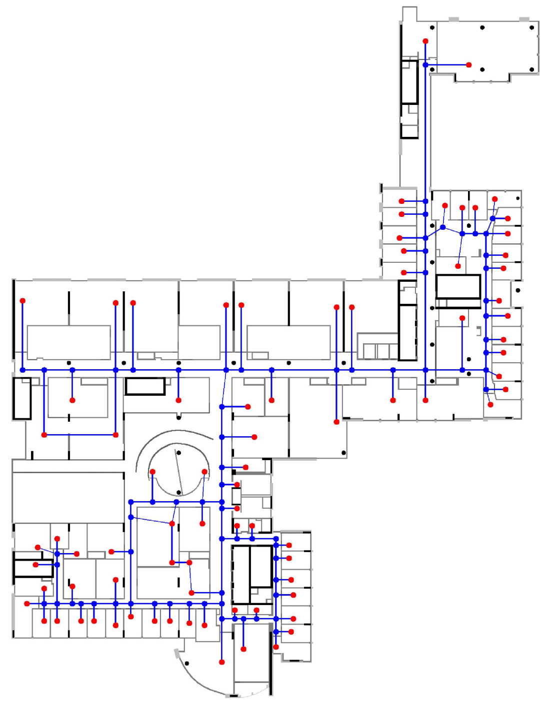

(b) CM model mobility graph superimposed on the Bahen's fifth floor blueprint.

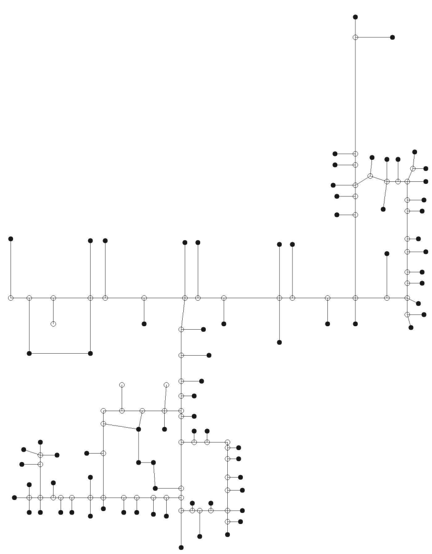

(c) Stand-alone CM model mobility graph.

Figure 4.1: From the AutoCAD blueprint to the CM model mobility graph.

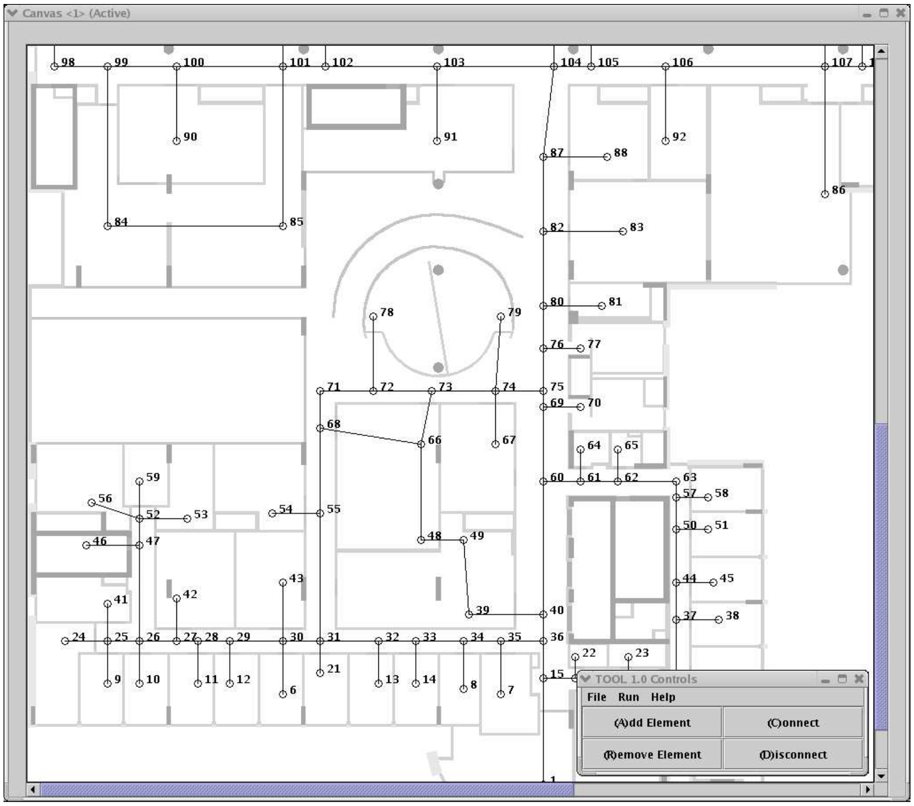

Figure 4.2: Graphical editor used to generate CM mobility graphs.

The CM model addresses node behavior in a simple way: we limit the choice of destinations to the set of red-colored vertices in the graph, situated in “interesting” locations such as offices, classrooms and conference rooms. Each node randomly chooses a vertex in this set, and moves toward it at a randomly selected speed. After reaching its destination, the node pauses for a fixed time period before resuming movement. We adopted this generic – and familiar – approach to behavioral mobility modeling because the main focus of our research is the modeling of physical obstacles constraining node movement.

CM does not yet account for smaller obstacles, such as furniture or the presence of other people/mobile nodes. We will revisit these issues when describing our future research plans.

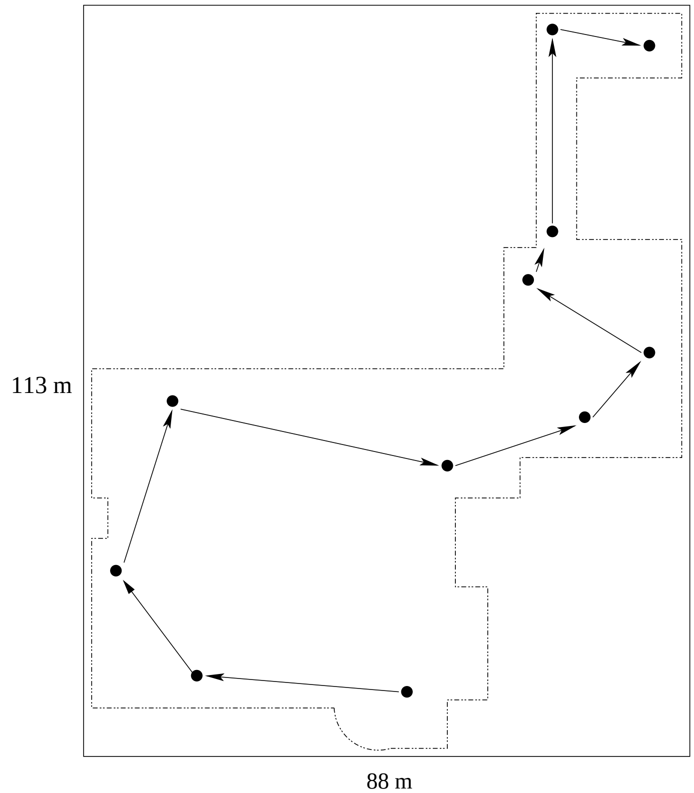

Figure 4.3: Mobility pattern of a node under Shell Mobility.

4.1 Simplifications to Mobility: Shell and RWP

The CM model we have described takes both internal and external walls into account. The *Shell Mobility* model is an initial simplification that discards the internal walls of the building and the mobility graph; instead, nodes select destinations randomly within the area outlined by the external walls of the building, and follow straight-line trajectories to their destinations. Shell thus increases the number of possible destinations, and distributes them uniformly. However, choice of destinations is constrained to locations that will not force nodes to step outside the floor plan perimeter. Figure 4.3 illustrates the mobility pattern of a node using the Shell model.

Discarding the external walls from the Shell model yields the Random Waypoint (RWP) model. We consider two variants of RWP. In the RWP_S (*small*), nodes move within a square with 73.5 meter sides; the area of this square is equivalent to the inhabitable area of the Bahen's fifth floor, and consequently the area where node movement takes place in the Shell and CM

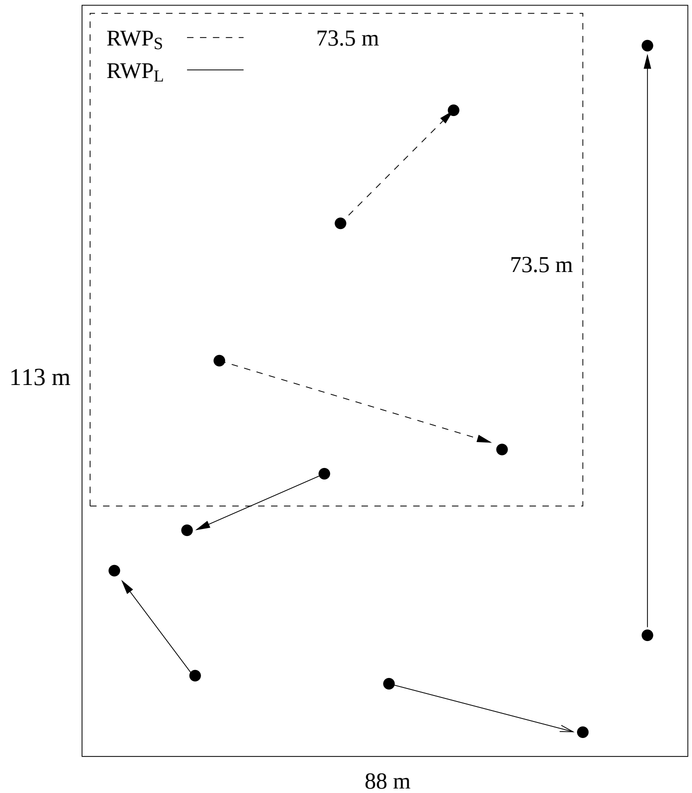

Figure 4.4: Node mobility under both variants of the RWP model.

models. In RWP$_L$ (*large*), nodes move in a rectangle of 113 by 88 meters, the area of the lot over which the Bahen building stands. Figure 4.4 illustrates the differences between both variants of the RWP mobility model.

4.2 Mobility Model Implementation

RWP mobility patterns can be generated for simulations in ns2 using *setdest*, a small independent application provided by the Monarch Wireless Extensions. *setdest* generates an OTcl script specifying node movement, which is fed to the simulator during setup time. The parameters needed by *setdest* to generate a RWP mobility pattern are: simulation time, number of nodes, rectangular dimensions of the simulation area, P and V_{max} (V_{min} is fixed at 0 m/s).

The mobility models we have described were implemented by extending the *setdest* program. To generate a CM mobility pattern, a text-based intermediate representation of a mobility graph is exported by our graphical editor and passed to the *setdest-cm* program. The control flow of *setdest* is altered: choice of destinations is limited to the distinguished vertices contained in the mobility graph specification, and a shortest path algorithm is used to find the path in the mobility graph that a node will use to move toward its destination.

To generate Shell mobility patterns, *setdest-shell* is given a specification of the outer perimeter of the floor plan under consideration. Whenever a node destination is chosen, the resulting trajectory is checked; if the node will step outside the outer shell of the building, the current choice is replaced by a new destination. Finally, all versions of *setdest* were modified to consider a V_{min} of 0.5 m/s, to avoid the average speed decay phenomenon reported by [27].

Chapter 5

Attenuation Factor Propagation Model

Attenuation Factor (AF) [55, 56, 30] is an empirical radio propagation model for indoor environments that deterministically accounts for multiple obstacles. AF models a time-invariant channel where the obstacles blocking the primary ray – the straight-line trajectory between the transmitter and receiver –, are responsible for the majority of the loss in signal strength perceived by the receiver. The remainder of the signal strength attenuation in AF is a function of the distance that separates the communicating nodes. While AF neglects propagation effects like reflection, diffraction and scattering, and only models obstacles after their material types but not their thickness or other characteristics, it has been shown to yield good accuracy and high computational efficiency [55]. To the best of our knowledge, this is the first application of AF to MANET simulations.

The AF model is given by Equation 5.1

$$P_{AF}(r, m_1, \ldots, m_\sigma) = P_o(r_o) - 10n\log_{10}\left(\frac{r}{r_o}\right) - \sum_{i=1}^{\sigma} m_i \cdot PF_i, \tag{5.1}$$

where P_o is the power at some nearby reference distance r_o, n is the path loss exponent that determines the rate at which power decreases with distance r, m_i is the number of obstacles of material type i along the primary ray path, PF_i is the partition factor loss due to material type i, and σ is the number of distinguishable material types ($1 \leq i \leq \sigma$).

To be able to use the AF model, we need to specify the values of its parameters: P_o, n, σ and the PF_is. These parameters are site-specific empirical approximations derived from experimental measurements. We next describe the equipment used and methodology followed to derive these quantities.

5.1 Measurement Equipment

Our measurement equipment consisted of two laptops running Linux Red Hat 9, kernel version 2.4.24, with Wireless Tools [57] enabled. Each laptop was equipped with an Enterasys Roamabout PCMCIA network interface card [58], based on the Orinoco 802.11b chipset and configured in ad hoc mode. The cards where attached to a special external omni-directional antenna [59] that provided a gain of 9 dBi, and a horizontally-shallow radiation pattern that minimized the effects of reflection on the floor and ceiling — only 11 degrees of vertical aperture. At 2 Mbps, the Enterasys network interface data sheet indicates a nominal transmit power of 15 dBm and a nominal sensitivity threshold of -91 dBm, guaranteeing a Bit Error Rate of less than 10^{-5}. With a cumulative gain of approximately 17 dB (two 9 dBi antennas minus pigtail losses), the setup was capable of recording signal strength values of -108 dBm for equivalent isotropic (0 dBi or unity-gain) antennas.

5.2 Site-specific Parameterization

We recorded 250 measurements of signal strength over the floor plan illustrated in Figure 5.3(a). Each trial involved three steps. First, the two laptops were randomly positioned on different locations corresponding to vertices of the mobility graph. Second, an attempt was made to establish communication between the two laptops. If successful, both laptops were configured to ping each other; otherwise, a new pair of vertices was chosen. Finally, when successful, both laptops simultaneously recorded signal strength values over a period of one minute. The granularity for the signal strength measurement provided by the card driver and the Wireless Tools was 1 dBm. The signal strength value was refreshed every time a new ping packet was received; each laptop recorded roughly 30 measurements for a given pair of locations. We set the signal strength to the average of the measurements from both laptops. In the appendix of this thesis we report the values recorded by these empirical measurements.

Given stationary measurements and the symmetry of our experimental setup, we expected both laptops to record approximately the same signal strength values per trial, because of the electromagnetic principle of *reciprocity* [60]. We did not anticipate the large effect the movement of other people would have on the assumption of a time-invariant channel: to achieve reciprocity, measurements had to be taken late at night. This is a clear example of the importance of modeling small scale fading channels; in section 7.2, we will illustrate how this crucial feature is neglected by many other radio propagation models. Adding a small scale fading component to the AF model is thus our main future research goal for this part of our project — we will comment more on this in chapter 8.

To obtain the site-specific values for P_o, n and the PF_is we ran a regression test in MATLAB. For each measurement point k, we provided MATLAB with the measured signal strength $\bar{P}_k$, the distance r_k from the transmitter, and the number of walls of each type m_{ik} between the transmitter and the receiver. We then instructed MATLAB to iteratively minimize the error between the empirical measurement and the value predicted by the AF function; we used two different estimators (least-squares and Lorentzian), and considered different numbers of materials ($\sigma = \{1,3,4,7\}$).

We could distinguish seven material types in our AutoCAD floor plan: exterior walls, interior walls, exterior glass, interior glass, steel, concrete, and wood. However, the best fit to the empirical measurements involved only four materials (σ=4). The interior walls and wood were combined into one material (PF_1=2.479 dB), metal and steel into another (PF_2=4.7727 dB), interior and exterior glass into a third (PF_3=3.11104 dB); exterior walls were our fourth material (PF_4=6.50076 dB). The effect of furniture and smaller obstacles was accounted for by

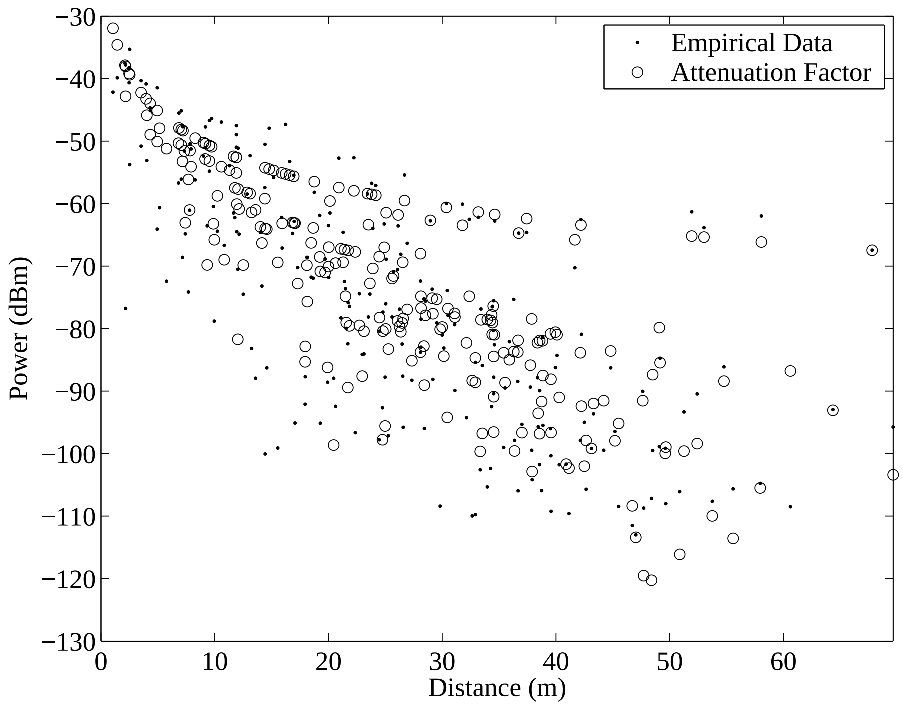

Figure 5.1: Signal strength measurements and AF fit. Each measurement (dot) is paired to its AF approximation (bubble) in the same vertical axis.

n and P_o, which were fit to 1.9665 and -31.4627 dBm, respectively. r_o was nominally set to one meter. The resulting AF parameterization (the circles in Figure 5.1) presents an average relative error of 8.9% with respect to the experimental data. In Figure 5.2 we plot the cumulative distribution function of the relative errors of the AF fit with respect to the empirical measurements.

Figures 5.3(b) and 5.3(c) show an AF-generated visualization of the signal strength of a transmitter placed in the center of the floor plan depicted in Figure 5.3(a), and illustrate the dramatic effect of wall attenuations on signal strength. The sensitivity threshold employed in this visualization is the default Enterasys value of -91 dBm.

In its present state, AF shares many of the simplifying assumptions of other propagation models, such as a two-dimensional topology, omni-directional antennas and a time-invariant channel. Overcoming these limitations is a subject for future work.

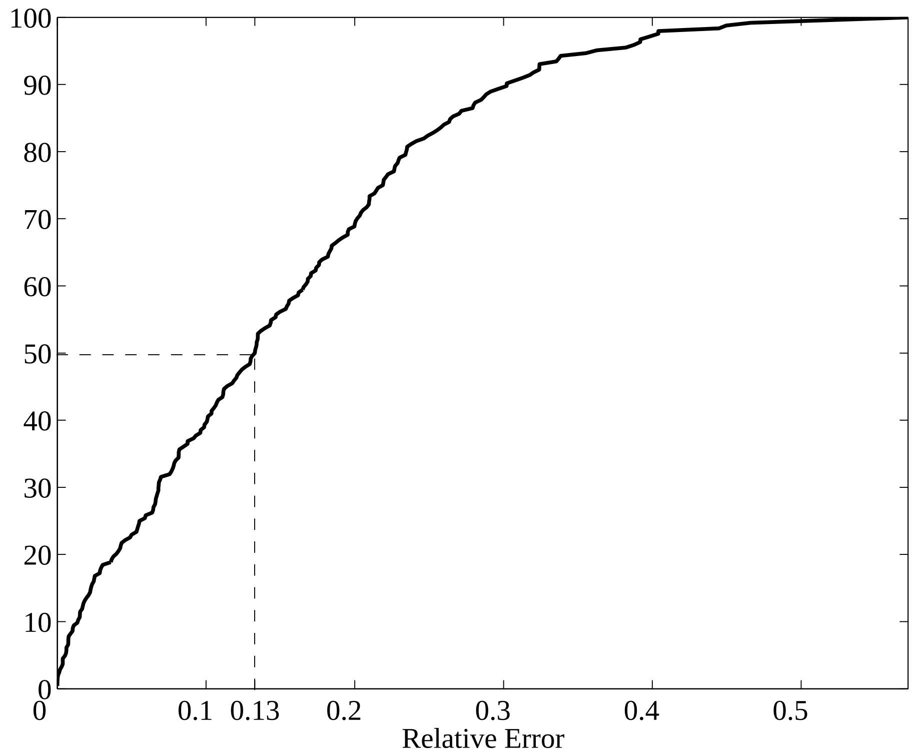

Figure 5.2: Cumulative Distribution Function of the relative errors of the AF fit with respect to the empirical measurements. The median of the relative error falls at 0.1328.

5.3 Simplifications to Radio Propagation: FS and Line-Of-Sight

A natural simplification to the AF model is to remove the explicit consideration of obstacles. The Free Space (FS) model usually employed in MANET simulations does this by assuming that signals propagate though a vacuum. This is an inappropriate assumption for our indoor environment: for the output power and sensitivity thresholds of typical WiFi 802.11b hardware, such as the one used to parameterize the AF model[1], any single node will obtain full radio coverage of the network.

To obtain a realistic basis for comparison with AF, we need to scale down the effective

[1]An output power of 15 dBm, a frequency of 2.4 GHz and a sensitivity threshold of -91 dBm at 2Mbps.

(a) Blueprint of the fi fth fbor of the Bahen Centre for Information Technology.

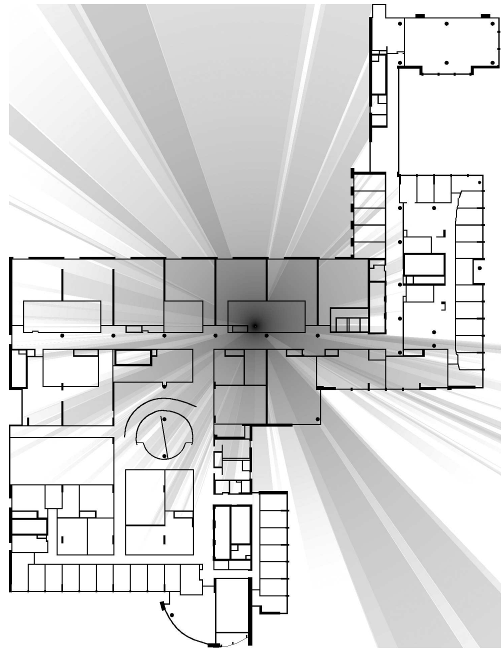

(b) Coverage pattern of a transmitter placed in the center of the Bahen's fi fth fbor, superimposed on the blueprint.

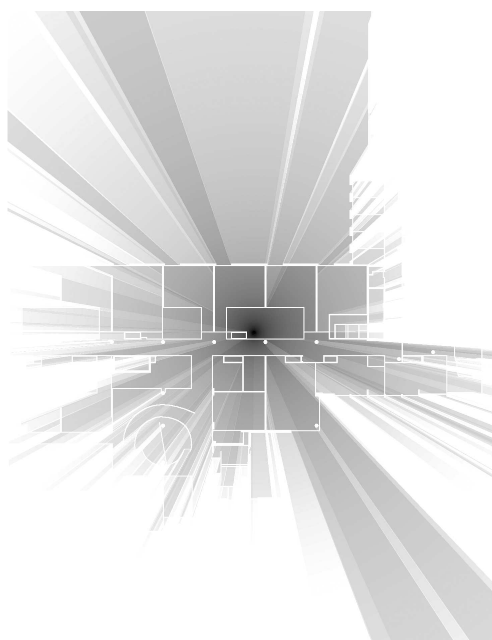

(c) AF coverage for a transmitter placed in the center of the Bahen's fi fth fbor.

Figure 5.3: From the AutoCAD blueprint to the AF implementation.

communication range of FS. The problem resides in finding a suitable approximation for the communication range in AF propagation: remember that this value is a function of the sensitivity threshold in propagation models that establish a one-to-one relationship between power and distance — not the case of AF. To solve this problem, we employ the Log-Distance Path Loss (PL) function given by Equation 5.3 (in dBm). This function is a generalization of FS (revisited in Equation 5.2), where we assume an arbitrary homogeneous medium characterized by a path loss exponent n. As in the AF model, P_o is the reference power at some nearby distance r_o. Note that AF can be seen as a generalization of PL, as well: in the PL equation all the attenuation factor (the PF_i's) are set to zero.

$$P_{FS}(r) = P_o(r_o) - 20\log_{10}\left(\frac{r}{r_o}\right) \tag{5.2}$$

$$P_{PL}(r) = P_o(r_o) - 10n\log_{10}\left(\frac{r}{r_o}\right) \tag{5.3}$$

We used MATLAB to fit the PL equation to our empirical measurements, using the same process we employed to parameterize the AF model. The best fit for the PL function, yielding a 14.85% relative error, corresponds to $n = 4.0602$ and $P_o = -19.2464$ dBm, for a nominal reference distance r_o of 1 m. This fit is plotted in Figure 5.4 as a dashed line. Note that the path loss exponent (n) obtained roughly corresponds values reported in the bibliography [55, 17].

The PL fit we obtained offers a reasonable set of communication ranges for comparison against AF. This is shown in Table 5.1: for a set of sensitivity thresholds employed in AF propagation (the thresholds start from the default Enterasys value of -91 dBm, and then increase by 10 dB at a time), we can see the corresponding PL effective communication ranges. These communication ranges are then applied to the FS propagation function, and the corresponding sensitivity threshold needed to yield those ranges are shown in the last row; note how the thresholds need to be downscaled to obtain a fair comparison with AF. We employed in our simulation analysis the resulting site-specific downscaled FS model, which we will refer to as FS′.

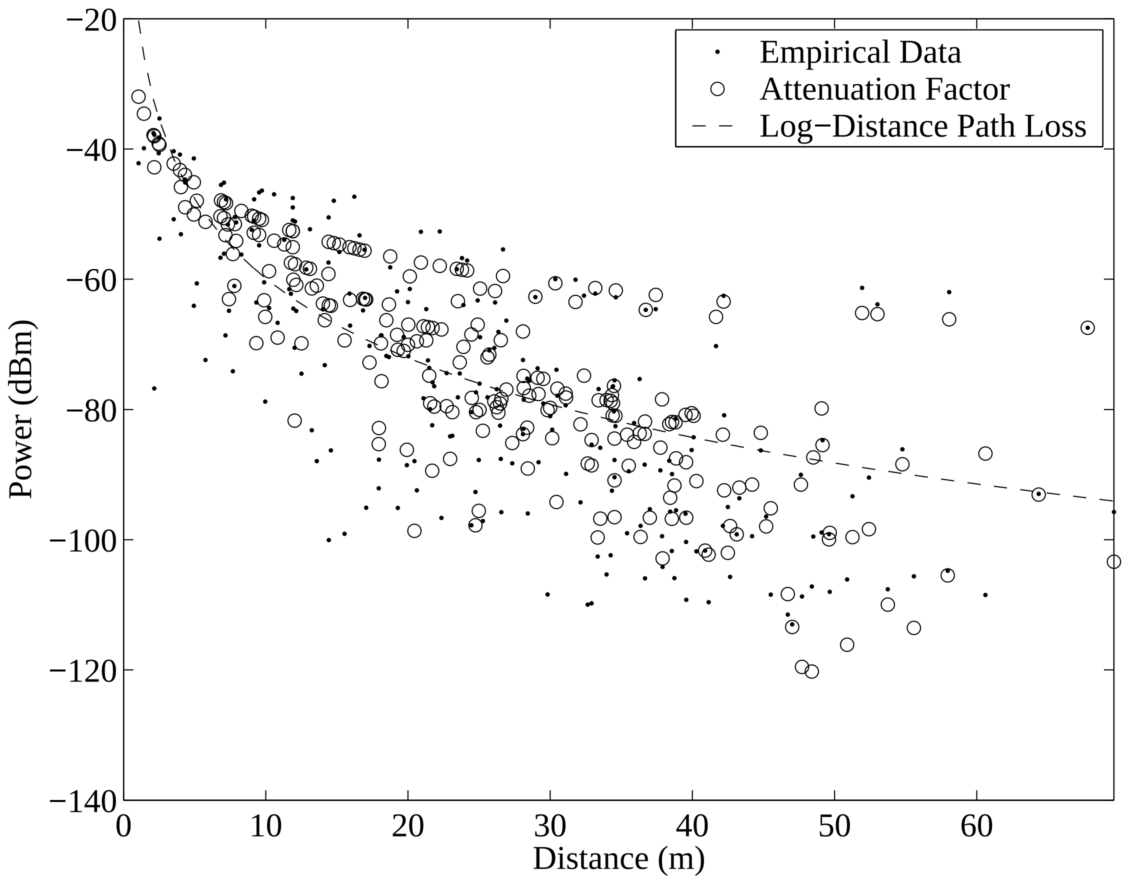

Figure 5.4: Signal strength measurements and PL fit. Compare to AF fit.

AF Threshold (dBm)	-51	-61	-71	-81	-91
PL Range (m)	6.05	10.67	18.82	33.19	58.51
FS′ Threshold (dBm)	-10.68	-15.6	-20.53	-25.46	-30.39

Table 5.1: PL effective communication ranges for different AF sensitivity thresholds, and corresponding FS′ sensitivity thresholds.

The second simplified propagation model we consider is Line-Of-Sight (LOS) propagation. This model has been previously used in MANET simulation [8, 14]. It is a basic extension to Two-Ray Ground where two propagation conditions are differentiated: if any obstacle obstructs the primary ray between transmitter and receiver, connectivity between the nodes is preempted; otherwise, there is a clear line of sight propagation path and conventional Two-Ray Ground propagation is assumed.

Figures 5.5 presents visualizations for FS and LOS propagation, which serve as useful illustrations of the differences between the models — compare to the AF visualization in Figure 5.3(c). In the absence of reflection, diffraction and the scattering effects of multi-path propagation, we can view the three propagation models considered as coexisting in the same axis (Figure 5.6). While FS assumes the attenuations to signal strength due to obstacles in the primary ray to be always zero, LOS is the exact opposite, as it models infinite attenuation by any obstacle. AF propagation stays in between, and adds another level of sophistication by considering different attenuation factors for different materials.

5.4 Propagation Model Implementation

An implementation of the FS model is bundled with the ns2 network simulator, along with implementations for other propagation models, such as Two-Ray Ground. We have created two additional radio propagation classes for the AF and LOS models.

Our implementation of the AF model is capable of determining the perceived power at

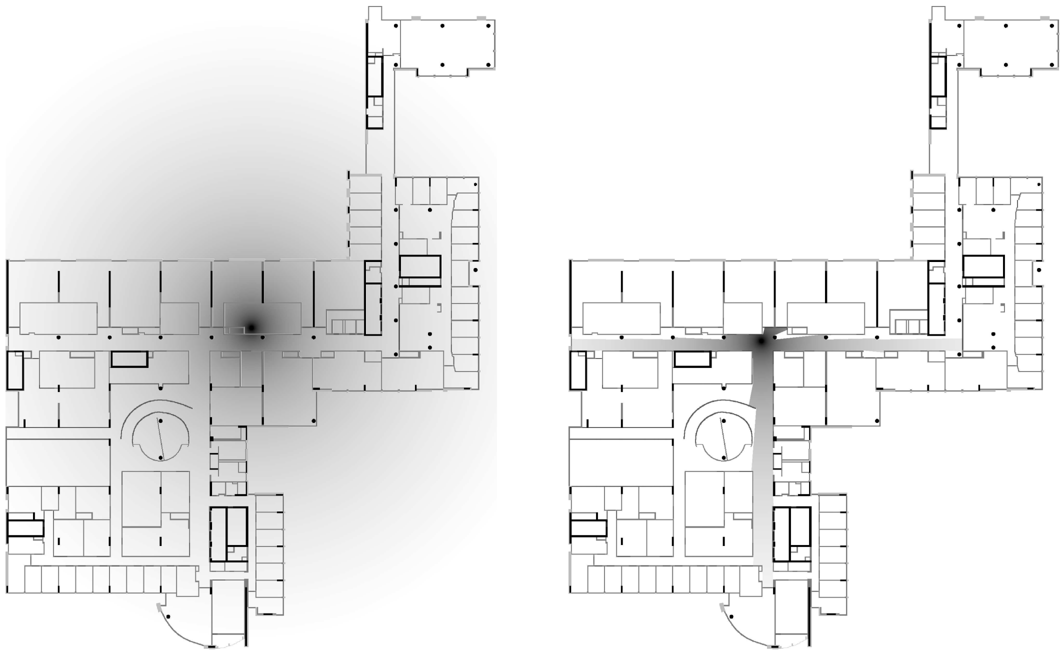

(a) Free Space. Effective transmission range is 58.51 meters. Transmitter in the center of the fbor plan.

(b) Line-Of-Sight. Notice that the transmitter was moved to a different position in the fbor plan.

Figure 5.5: Visualizations of simplified propagation models.

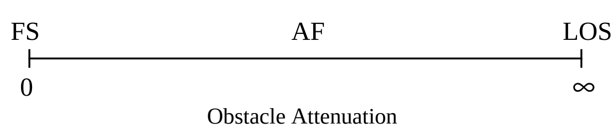

Figure 5.6: Conceptual comparison of the three propagation models under consideration.

the receiver for any pair of nodes arbitrarily positioned inside the modeled floor plan. The distance r between the nodes is computed, and the number of walls of each type obstructing the primary ray (m_i, $1 \leq i \leq \sigma$) is determined using the environment's AutoCAD floor plan. The signal strength perceived by the receiver is obtained by using Equation 5.1 with the empirically derived parameters, and the computed input values.

Our implementation of the LOS model is inherently much simpler. The same algorithm employed in AF to determine the number of walls obstructing the primary ray is used to determine line-of-sight connectivity between transmitter and receiver. If there is no line of sight, connectivity is disallowed; otherwise, the distance r between the nodes is computed, and the Two-Ray Ground propagation method is onvoked to determine signal strength — note that for the typical indoor environment Two-Ray Ground reduces to Free Space.

Chapter 6

Experimental Evaluation

In this chapter we present the results of our analysis on the robustness of simplified simulation models for MANET evaluation. To conduct this study, we employed several combinations of the mobility and radio propagation models presented in chapters 4 and 5. We compared the effects induced by the successive simplifications in the perceived performance of different routing protocols; our main objective was to establish if any simplification is suitable as a reliable trend illustrator, i.e. if any of the simplifications can be deemed robust. The chapter is organized as follows: section 6.1 describes the simulation environment and parameters. Section 6.2 describes the simulation methodology and metrics considered. Section 6.3 presents the main results obtained, and section 6.4 explains the reasons for those results. Finally, additional closing remarks are presented in section 6.5.

6.1 Simulation Environment

We ran our experiments using the *ns2* [17] network simulator version 2.26, augmented with the Monarch Wireless Extensions [18]. We employed the implementations of the DSR and DSDV routing protocols provided by the Monarch extensions, with the constants listed in tables 2.1 and 2.2, respectively. We also used the Wireless Extensions' implementation of the 802.11 DCF MAC protocol, as well as the FS and RWP models. As previously explained, we implemented the CM and Shell mobility models, and the AF and LOS propagation models. We also instrumented the simulator to obtain the metrics described in section 6.2.

We report results for networks of 20, 30, 40, 50 and 60 nodes. All experiments ran for 1200 seconds of simulated time. We simulated wireless communication at a frequency of 2.4 GHz, with a channel capacity of 2 Mbps, compatible with the 802.11b standard. In all simulations, nodes choose a speed uniformly distributed between 0.5 and 3 m/s, which we regard as the range of human walking speeds in an indoor environment. To provide a highly dynamic scenario and stress the routing protocols, we set the pause time to zero seconds on all simulations.

We modeled network traffic using Constant Bit Rate (CBR) sources. A CBR traffic source provides a constant stream of packets throughout the whole simulation, thus further stressing the routing task. In each experiment, half the nodes in the network are CBR sources, and each source transmits 64-byte packets at a rate of 4 per second. We experimented with higher sending rates, packet sizes and number of sources. We omit those results, as they show similar trends, with the predictably higher effect of network congestion.

We experimented with a variety of sensitivity thresholds for the AF model, ranging from the default value of -91 dBm described in the Enterasys NIC specification, up to -51 dBm, with a step of 10 dBm. Varying the sensitivity threshold is equivalent to varying the transmission output power, and determines the degree of connectivity of the network. Based on the mappings from Table 5.1, we experimented with FS′ effective communication ranges between 5 and 60 meters. By definition, the LOS model reflects a coarse-grained binary propagation condition, hence we only consider a very high sensitivity threshold that will allow connectivity in a line-of-sight situation, regardless of the distance.

All the results presented are averages of five runs over different randomly generated mobility patterns. For all experiments, no significant variance was observed among different runs for the same scenario; standard deviation values were consistently smaller than 10% of the corresponding average.

6.2 Simulation Methodology

In this thesis we regard the Constrained Mobility (CM) and Attenuation Factor (AF) models as the baseline against which we compare the robustness of simplified simulation models. We first compare CM-AF against the other less detailed propagation models, LOS and FS′. Once we have removed the deterministic consideration of obstacles from the propagation model, we also consider mobility models which gradually neglect obstacles: first the Shell model and then the two variants of RWP, $\mathrm{RWP_S}$ and $\mathrm{RWP_L}$.

Note that in the following sections, the LOS propagation model is briefly analyzed separately, as it quickly demonstrates to be a very inaccurate alternative for indoor MANET simulation.

The robustness of the simplified models we consider is characterized by their impact on the routing protocols' performance. We employ two protocols, DSR and DSDV, and evaluate them through the following metrics:

Packet Delivery Rate (PDR): the ratio of application layer packets that were successfully forwarded to their intended recipients by the end of the simulation. This is the main evaluation metric in MANET routing protocol research. Notice that since we use CBR sources with fixed parameters, the PDR is equivalent to the network throughput.

End-to-end Latency: for all delivered packets, the average time elapsed between generation at the sender and reception at the destination. This includes buffering in queues, transmission times, and delays waiting for successful MAC control exchanges and routing activity.

Routing Packet Overhead: the total number of routing packets transmitted during the simulation. This reflects the degree of routing activity, which is also sometimes characterized by the normalized routing load, i.e. the ratio of routing packets transmitted to application layer packets received.

The way we evaluate the PDR deserves further explanation. It is possible that a packet cannot be transmitted by its sender to the first hop of the route toward its destination, because the number of MAC layer CTS/RTS exchange retries was exceeded, due to congestion or other conditions. A routing protocol can then drop the packet definitely, or attempt a number of retransmissions. This represents a trade-off between delivery and latency: for some applications, such as streaming, it is preferable to lose a certain number of packets and have those that arrive do so in a timely manner; for other applications, such as ftp transfers, it is imperative to successfully deliver every packet, even if some packets take longer and have to be retried many times. In this thesis we have – rather arbitrarily – decided to favor the first scenario: if a packet is dropped by the MAC layer at the sender, it is not counted as a delivery failure. However, if the routing protocol does not drop the packet and attempts a retransmission, the packet is considered still deliverable, and if it successfully reaches a different node it will be accounted for in the PDR metric.

We further analyze the routing activity through other metrics, related to the internals of each protocol. For DSR, we quantify the number of routing packets of each type that were transmitted – Route Request, Route Reply, Route Error and Unknown Flow Error – and the number of packet salvagings that happened during the simulation. For DSDV, we determine a lower bound on the number of routing packets transmitted, obtained by applying the protocol constants to the particular experimental conditions of each simulation configuration. We employ this lower bound to better quantify the overhead incurred in by the routing task.

We also consider four topology metrics that are protocol independent. These metrics are evaluated off-line, not during simulation time but during mobility pattern generation. The values of these metrics are thus based on nominal propagation conditions and do not account for collisions or interference during packet transmission. The metrics reflect the combined effect of the mobility and radio propagation models on the network topology that the routing protocols see, and are therefore employed to explain the behavior of the protocols. Besides absolute values, we also report normalized values for two of these topology metrics.

Neighbor Density: the average of the number of peer nodes within connectivity reach for each node at any given time. We normalize the neighbor density by expressing it as a fraction of the maximum number of neighbors, $n-1$ for a network of n nodes.

Optimal Path Length: the average length in hops of the optimal path for those pairs of nodes for which a path actually exists, at any given time.

Link Changes Count: the average of the number of connectivity changes between each pair of nodes. We normalize the link changes count by expressing it as the fraction per link or node pair, $n*(n-1)/2$ for a network of n nodes.

Link Disconnection Time CDF: every time a link between two nodes break, we measure the period of time the link remains broken. We then report the Cumulative Distribution Function of the link disconnection times.

The values reported for the normalized topology metrics are those for a network of 40 nodes. Because of normalization, the results for networks of different sizes are practically identical.

6.3 Robustness of Simplified Simulation Models

Figures 6.1 and 6.2 show the PDR for the experiments we have conducted. The graphs do not include the results for LOS propagation; we leave that analysis for later. In Figures 6.3 and 6.4 we show the latency results for the same experiments. Note that the results for the two metrics are intimately related: lower delivery rates are coupled with almost exponentially higher latencies in packet delivery – the latency graphs have a logarithmic scale –. The relationship between both metrics will be analyzed in section 6.4.

A comparison of Figures 6.1 and 6.2 provides us with the first indication that simplifications of the mobility and radio propagation models may not be robust; the effects of the simplifications on performance are not uniform across the two protocols. While the perceived performance of DSDV does not seem to be affected in any way by successive simplifications of the simulation models, the performance of DSR varies widely across the different models. This result shows that conclusions reached about the relevance of detail in the evaluation of one MANET protocol may not carry over between protocols, and that assuming otherwise will likely produce misleading results.

For example, from the DSDV results it may be inferred that $\mathrm{RWP_L}$-FS′ – the simplest model under consideration, where no obstacles for mobility or radio propagation are accounted for – is a robust approximation of the significantly more complex CM-AF. The similar performance trends presented by the protocol under both models, and the fact that the results obtained with $\mathrm{RWP_L}$-FS′ are within a bounded and consistent error from the results yielded by the sophisticated model, seem to bolster this assertion. Unfortunately, if we were to evaluate DSR relying on $\mathrm{RWP_L}$-FS′ as our model, we would reach the erroneous conclusion that DSR outperforms DSDV, or at least matches its performance, in most cases. Note that the exact opposite occurs if we consider the more detailed model.

Figure 6.2 provides further evidence that simplified models are not robust: the relative performance of DSR under different models changes dramatically as we increase the number of nodes. For example, the protocol's performance under CM-FS matches the results obtained under $\mathrm{RWP_S}$-FS′ for 30 nodes (Figure 6.2(b)); however, as we increase the network size the apparent equivalence between both models vanishes, and for 50 nodes DSR under CM-FS is completely outperformed by the same protocol under the simpler model (Figure 6.2(d)).

Thus we draw our second conclusion: as we modify the experimental parameters, observations about the relevance of detail do not necessarily carry over even within the evaluation of the same protocol. For example, assume that a researcher is evaluating an energy-aware enhancement to DSR that attempts to reduce the energy consumption of the mobile nodes by diminishing the transmitter output power. The assumption is that network throughput should be sustained, or even increased, since by decreasing node connectivity more simultaneous communication flows could be potentially maintained in disjunct regions of the network [61, 62].

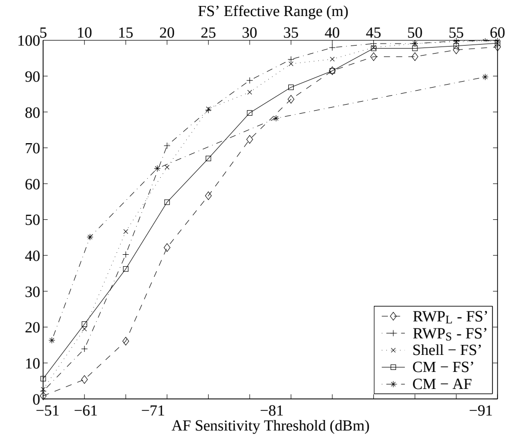

(a) 20 Nodes

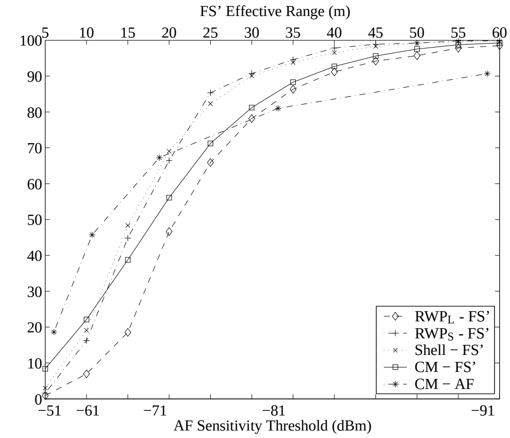

(b) 30 Nodes

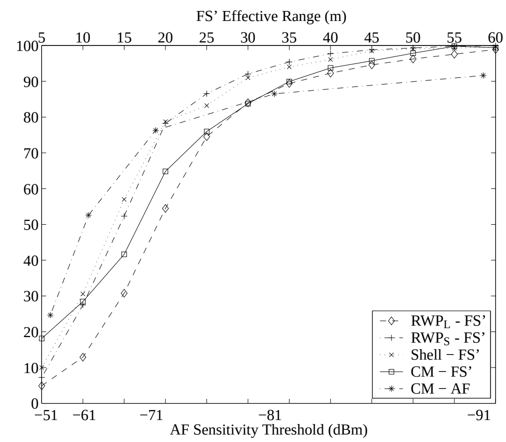

(c) 40 Nodes

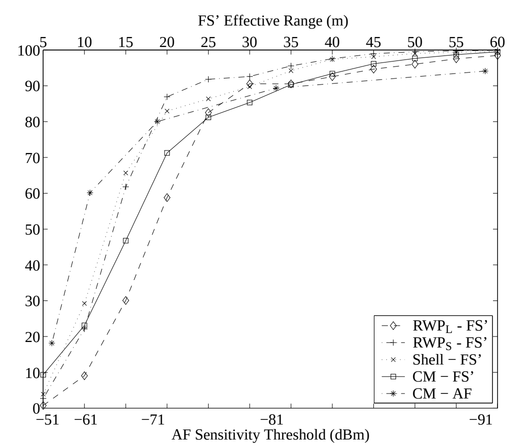

(d) 50 Nodes

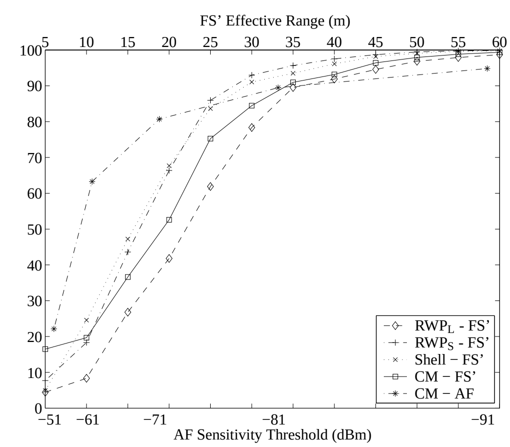

(e) 60 Nodes

Figure 6.1: DSDV packet delivery rate.

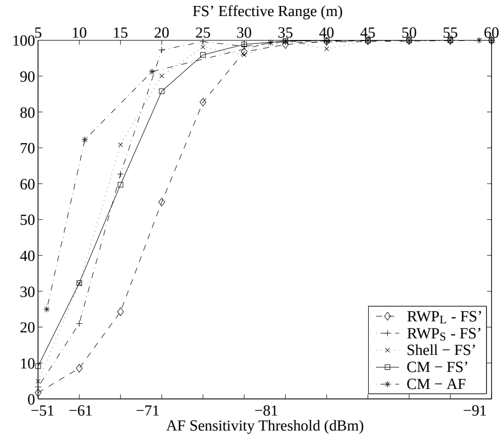

(a) 20 Nodes

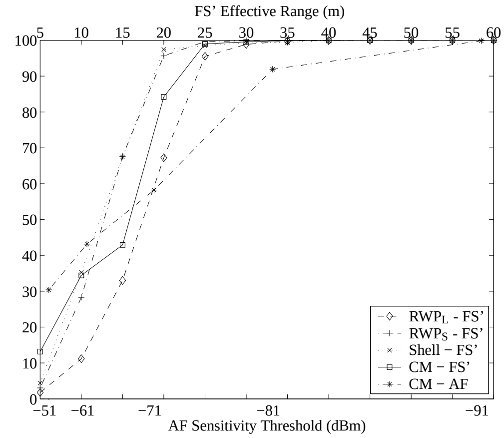

(b) 30 Nodes

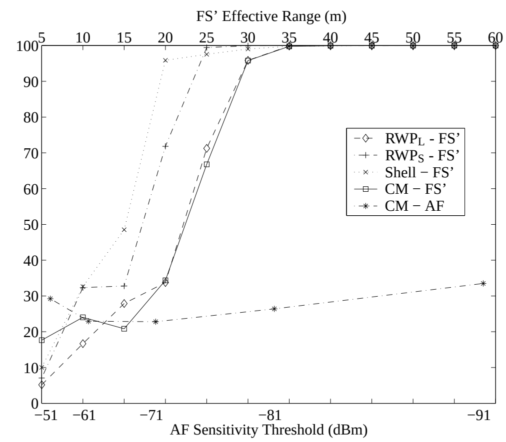

(c) 40 Nodes

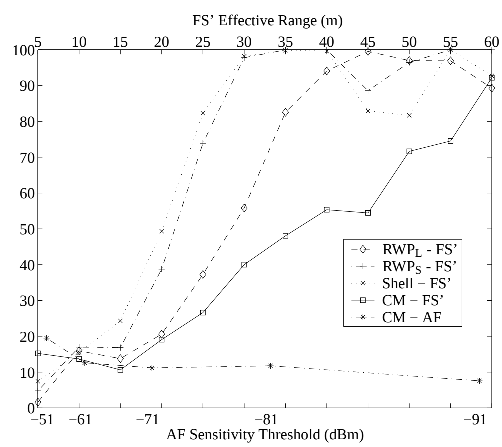

(d) 50 Nodes

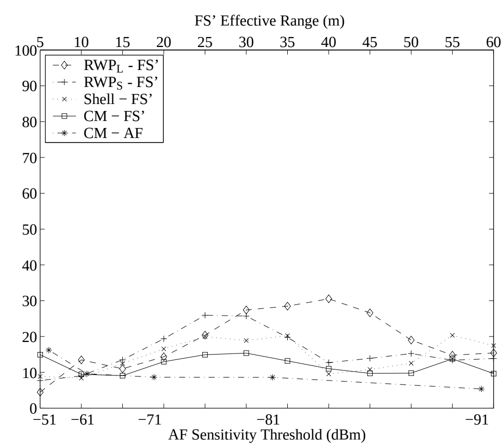

(e) 60 Nodes

Figure 6.2: DSR packet delivery rate.

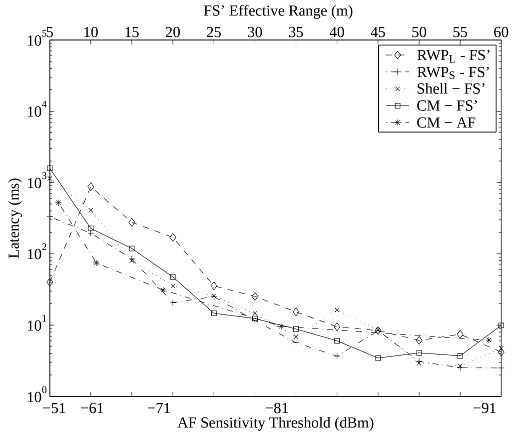

(a) 20 Nodes

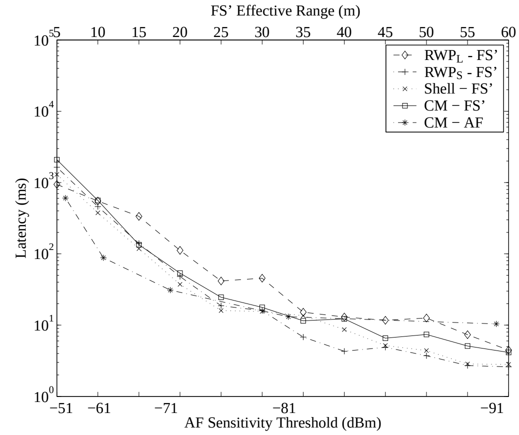

(b) 30 Nodes

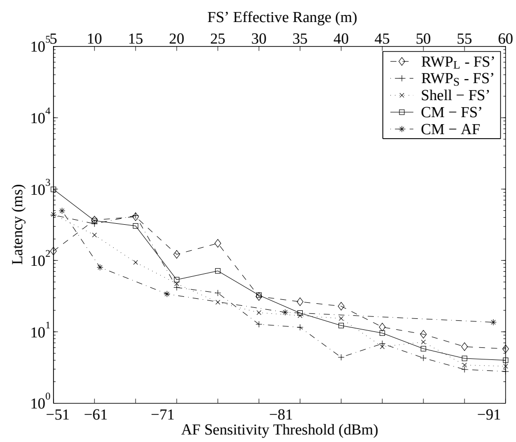

(c) 40 Nodes

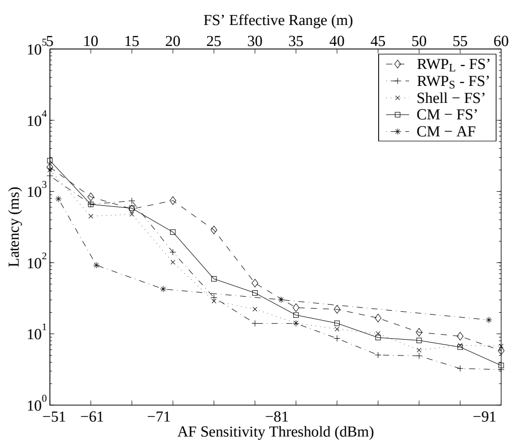

(d) 50 Nodes

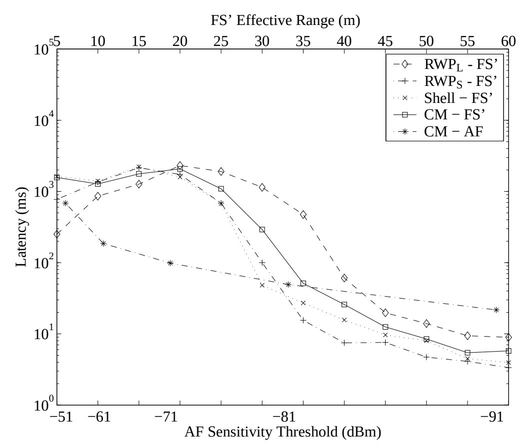

(e) 60 Nodes

Figure 6.3: DSDV packet delivery latency.

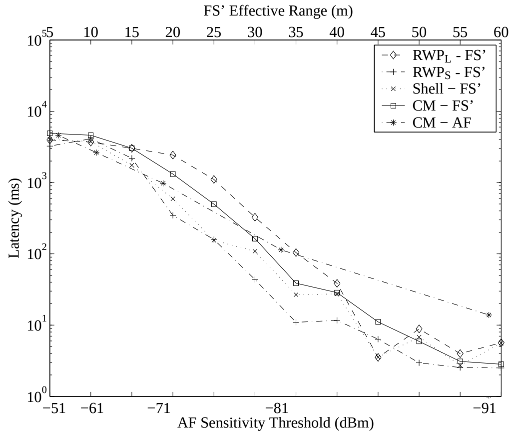

(a) 20 Nodes

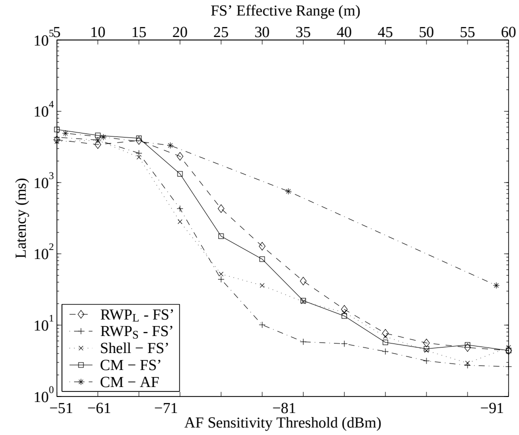

(b) 30 Nodes

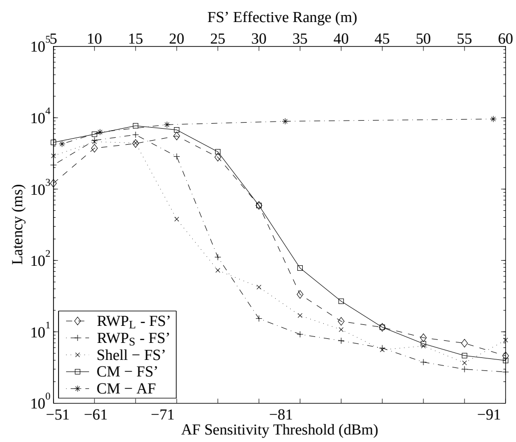

(c) 40 Nodes

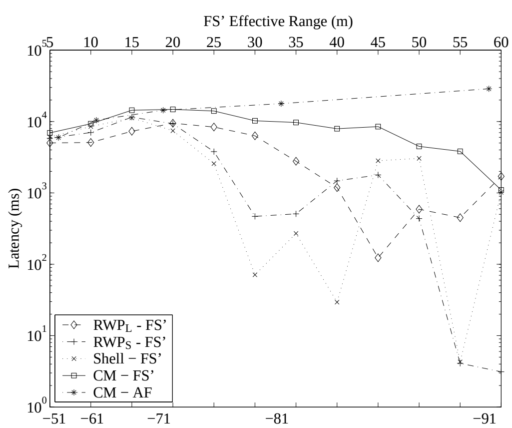

(d) 50 Nodes

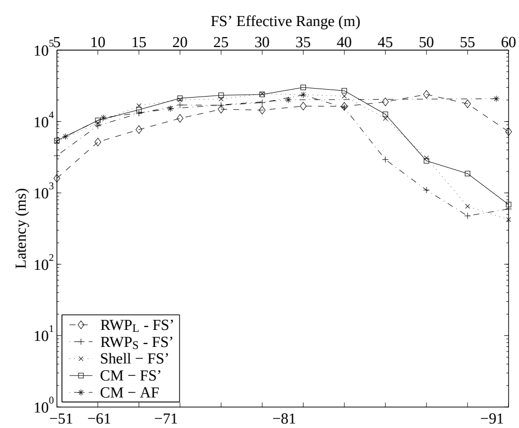

(e) 60 Nodes

Figure 6.4: DSR packet delivery latency.

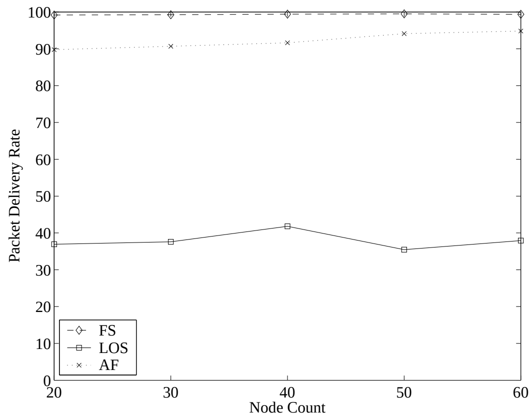

(a) DSDV

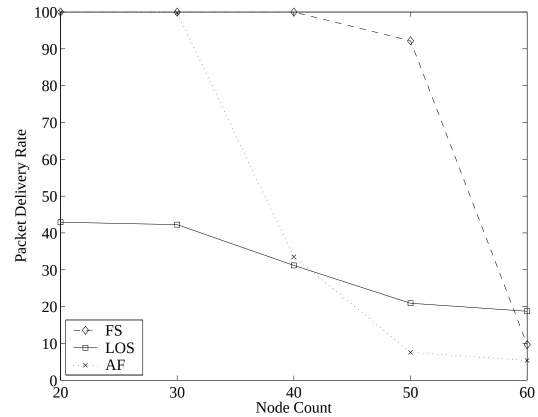

(b) DSR

Figure 6.5: Routing protocols performance under various propagation models, including LOS, for different network sizes. CM mobility employed.

Evaluation of this optimization under RWP$_S$-FS′ would lead to the false conclusion that for a network of 50 nodes san effective transmission range of 35 meters (roughly a 10 dBm output power reduction) achieves an optimal delivery rate, very close to 100%. In contrast, experiments with CM-FS′ show that at this transmission range, the average delivery rate is closer to 50% (Figure 6.2(d)), and the latency in packet delivery is an order of magnitude higher (Figure 6.4(d)). Therefore, the power adaptation policy would not be effective for this network.

Finally, Figure 6.5 illustrates the results obtained for LOS propagation. In the Figure we compare the delivery rate obtained with the CM mobility model under FS′, LOS and AF propagation; the transmission range for FS′ is set to 60 m, while the sensitivity threshold for AF is set to the roughly equivalent -91 dBm, according to table 5.1. The results clearly show the inadequacy of the Line-Of-Sight assumption for an indoor environment. Connectivity between nodes is mostly preempted by the considerable number of obstacles, and multihop paths for packet delivery are only found when nodes are opportunistically positioned in hallway intersections. Delivery rates are thus steadily lower than 45% for any network size, a completely different result from the trends presented under AF and FS′ propagation. We will therefore give the LOS propagation model no further consideration.

6.4 Performance Breakdown

Figures 6.6 and 6.7 show the routing overheads for DSDV and DSR, respectively, for the experiments we conducted in the previous section. Notice the intimate relationship between the routing overhead and the performance results for each experiment, the PDR and latency. The routing overhead of DSR grows exponentially, both as the number of nodes increases and as more sophisticated simulation models are employed, completely overloading the network and preventing successful packet delivery. Furthermore, packets spend most of their time waiting in the priority queues behind the routing packets, resulting in the dramatic latencies we have reported. In contrast, for DSDV the overhead increases modestly with the number of nodes, and there are also lesser overhead variations between the models. Through the use of protocol-independent topology metrics we will explain the reasons behind the observed routing behavior.

We start our analysis by looking into the neighbor density metric. Figure 6.8(a) plots the normalized neighbor densities for the models we have experimented with. We can see an interesting discrepancy between the neighbor density curves of CM-AF and CM-FS′. With a lower transmission power, the neighbor density values of CM-FS′ are initially lower than those reported for CM-AF; when no obstacles block the primary ray between transmitter and receiver, AF propagation can actually reach farther in zones like hallways and large conference rooms. However, for ranges greater than 25 meters, the situation reverses as the attenuation effects of multiple walls become the limiting factor in AF propagation. Notice how this was illustrated in Figures 5.3(c) and 5.5(a): in FS′ propagation, the radio coverage of a node is effectively a disk, while for AF propagation, the attenuations induced by multiple obstacles render a non-circular coverage zone. Thus, for the upper band of sensitivity thresholds, individual nodes in FS′ reach an almost complete network coverage (90%), but coverage of the network with AF propagation

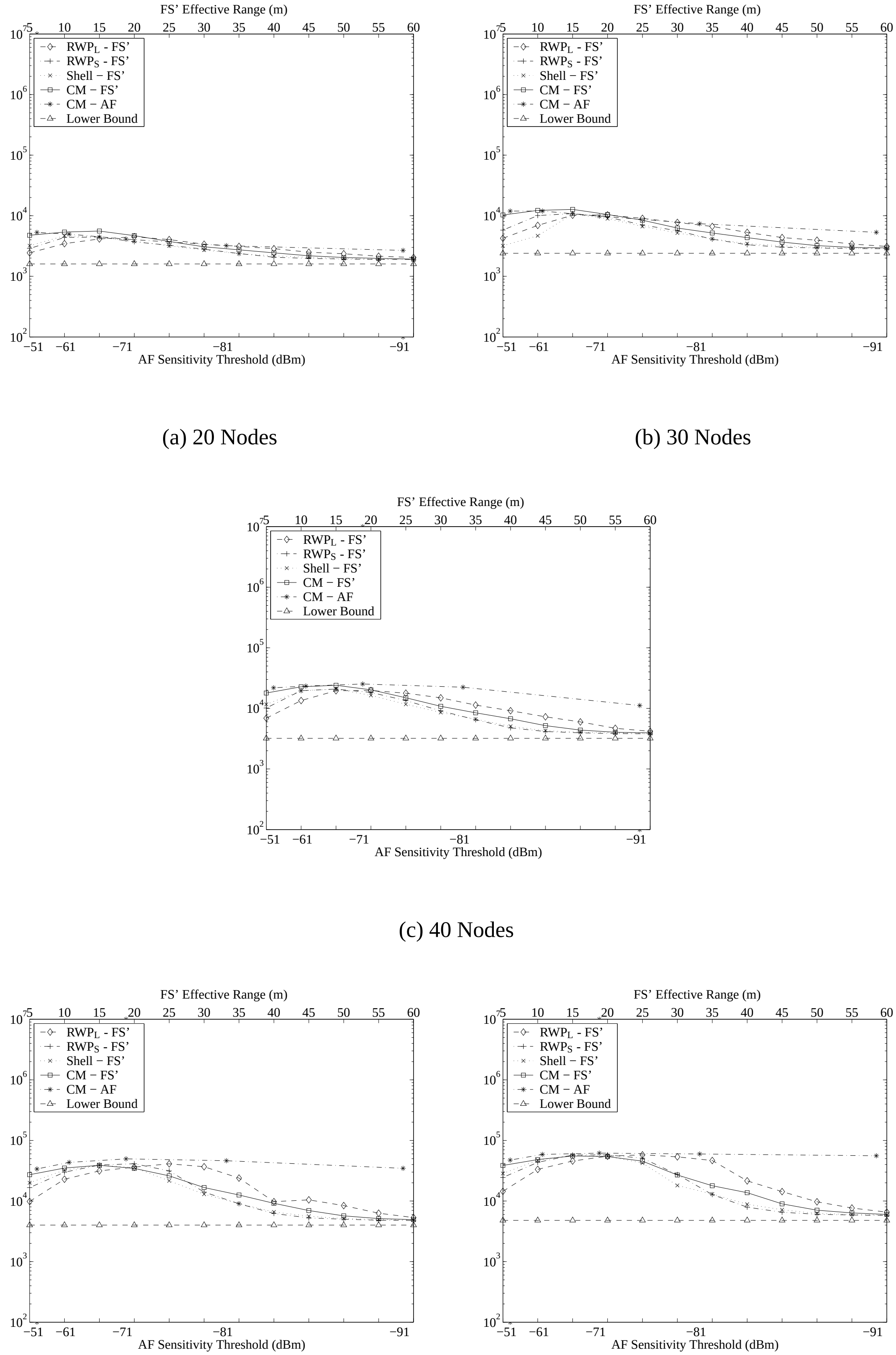

(a) 20 Nodes

(b) 30 Nodes

(c) 40 Nodes

(d) 50 Nodes

(e) 60 Nodes

Figure 6.6: DSDV routing packets overhead.

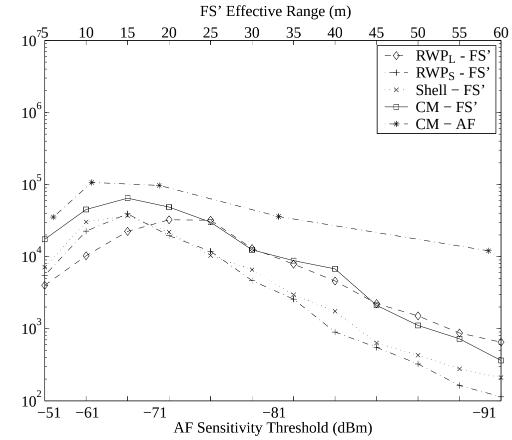

(a) 20 Nodes

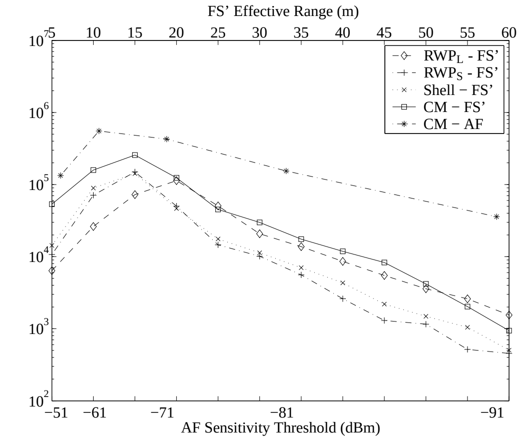

(b) 30 Nodes

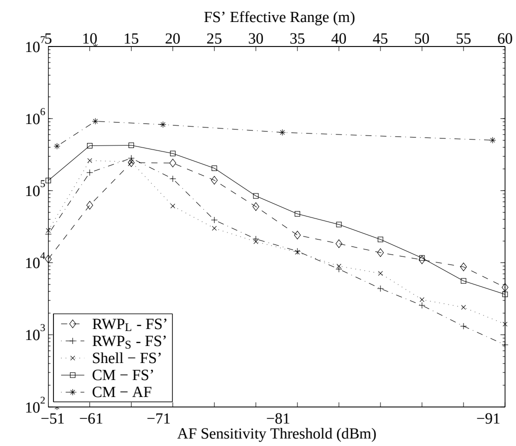

(c) 40 Nodes

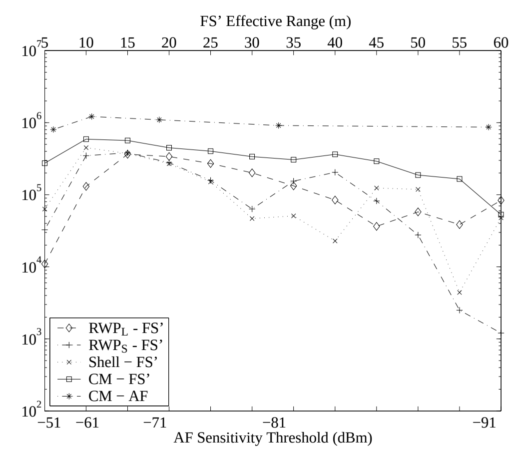

(d) 50 Nodes

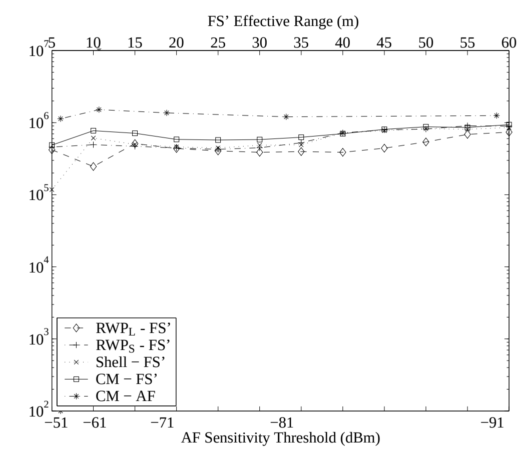

(e) 60 Nodes

Figure 6.7: DSR routing packets overhead.

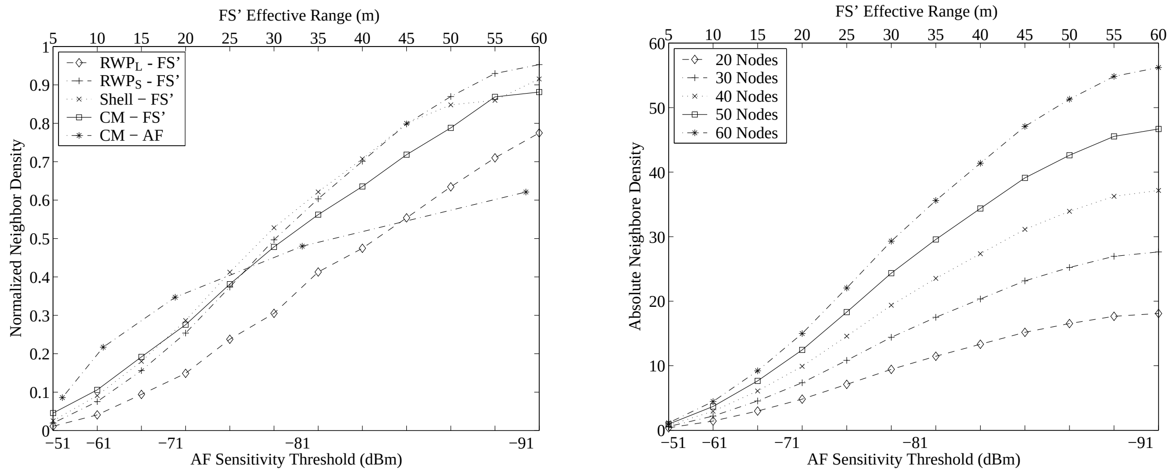

(a) Normalized neighbor density.

(b) Absolute neighbor density for RWP$_S$ mobility and FS′ propagation.

Figure 6.8: Neighbor Density.

is restricted to 62%. Figure 6.8(b) complements this analysis by showing the absolute neighbor densities under RWP$_S$-FS′, for networks of different sizes: notice the extremely high number of neighbors for the upper band of sensitivity thresholds.

A further analysis of Figure 6.8(a) shows that CM-FS′, Shell-FS′ and RWP$_S$-FS′ have similar neighbor densities. This result suggests that under FS′ propagation, neighbor density is mostly dependent on the effective movement area – which is equivalent for these three mobility models –, as opposed to the specific paths taken by nodes. RWP$_L$-FS′ models a larger space and has a consequently lower neighbor density.

The neighbor density values have a strong relationship with the results of the second topology metric we consider, the average optimal path length. Figure 6.9(a) shows that as the signal strength – and therefore neighbor density – increases, path length decreases; for example, as normalized neighbor density approaches the 100% mark, every node is within communication range of each other, and the network ceases to be multihop, yielding an average path length very close to one. Notice that for very low transmission powers, around -51 dBm, or the roughly equivalent five meters FS′ transmission range, the poor connectivity conditions result in actu-

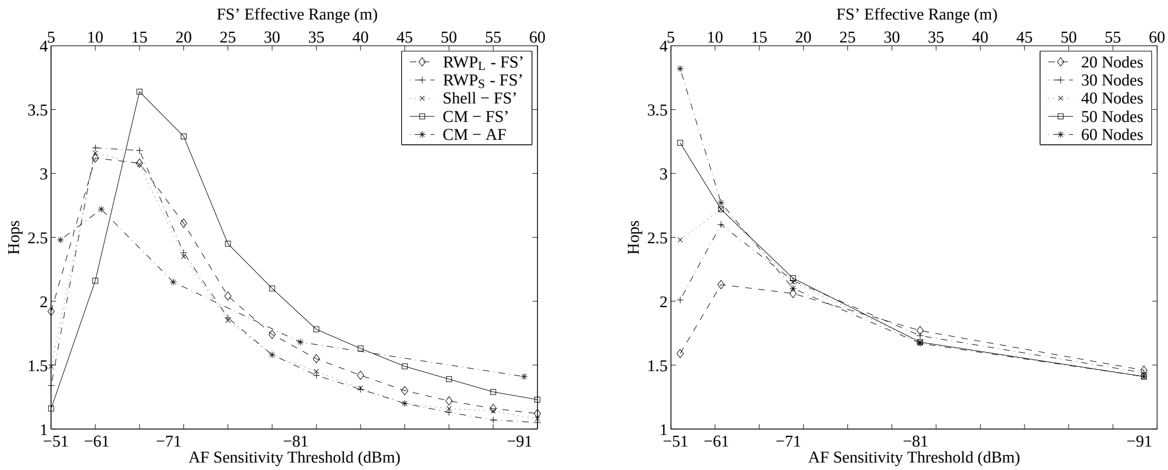

(a) Average optimal path lengths for a network of 40 nodes.

(b) Average optimal path lengths for networks of different sizes under AF propagation.

Figure 6.9: Average Optimal Path Length.

ally low average path lengths. Network partitioning isolates many nodes, and therefore fewer paths can be established, only between pairs of nodes positioned very close to each other. However, Figure 6.9(b) shows that as we increase the number of nodes the degree of node isolation diminishes, and thus the average path lengths fully correspond the neighbor density values. Finally, notice that the observed relationship between AF and FS′ propagation for the neighbor density metric is also present in the path length results.

At this point we can observe a very strong relationship between path length and routing overhead. For both protocols, longer paths imply more routing activity. In DSR, establishing longer paths translates to more retransmissions of route discovery messages, and a higher volume of route replies. In DSDV, the distance vectors of the different nodes take longer to stabilize into a globally consistent state, thus registering more intermediate stages in which changes in route metrics cause more triggered updates.

As the transmission power increases and the network becomes single hop, the routing task becomes trivial and routing overhead in DSR is negligible. For DSDV we see a similar scenario; notice that for this protocol we have plotted a lower bound on the routing activity derived

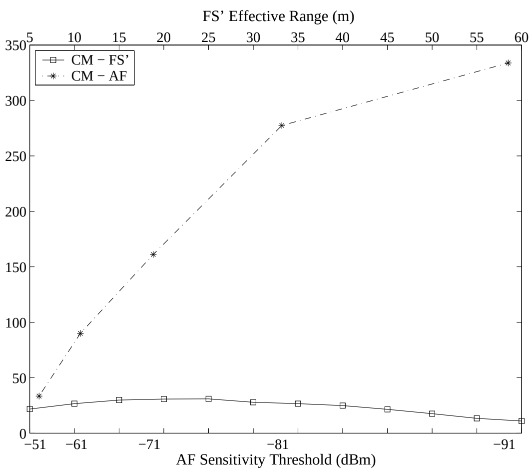

(a) Normalized link changes count for FS′ vs. AF propagation.

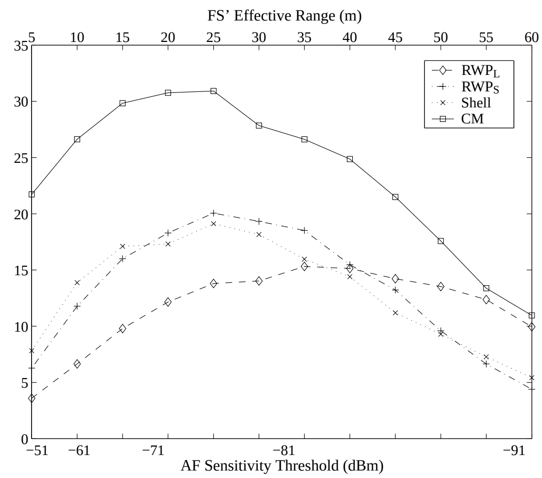

(b) Normalized link changes count under FS′ propagation.

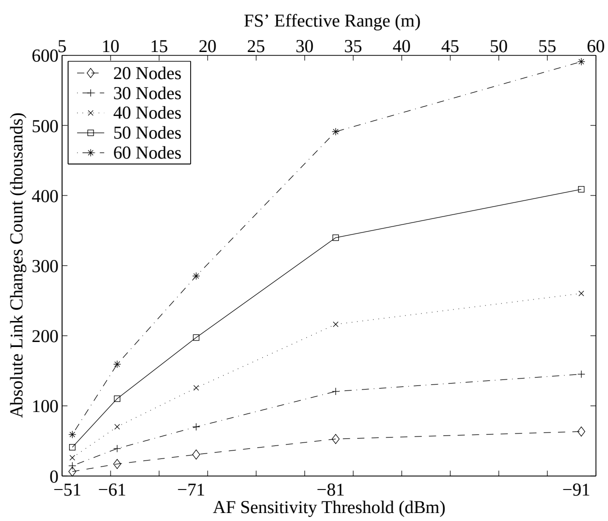

(c) Absolute link changes count for AF propagation.

Figure 6.10: Link Changes Count.

from the proactive component, the periodic updates. The lower bound determines the minimum number of packets that will be transmitted no matter what circumstances, and is given by Equation 6.1

$$\text{LowerBound}_{\text{DSDV}} = n * (T/\Delta), \tag{6.1}$$

where n is the number of nodes, T is the simulation time, and Δ is the full update period.

The previous analysis, however, fails to explain the overhead of both protocols under AF propagation. The routing overhead is consistently larger in all cases, disobeying the trend indicated by the path length values; moreover, for many scenarios it does not decrease with shorter paths. To explain this behavior, we turn our attention to Figure 6.10(a), which shows the most significant difference between AF and FS′ propagation: the dramatic difference in the number of link changes between both models. In CM-AF, the radio connectivity between two nodes suffers abrupt changes as the nodes move, since the corresponding primary ray is continuously obstructed by new obstacles. The sudden attenuations induced by the new obstacles result in numerous short disconnections. Figure 6.10(c) shows the overwhelming number of link breakages experienced under AF propagation in networks of different sizes.

In contrast, with FS′ propagation connectivity degrades slowly and smoothly as nodes move away, thus resulting in a much smaller number of link changes. Albeit smaller, there is a significant difference in the number of link changes between CM-FS′ and the other mobility models using FS′ propagation, as can be seen in Figure 6.10(b). In CM-FS′ nodes move away from one another much more quickly by traversing graph edges – walking through hallways – in opposite directions; this in turn causes a higher rate of link changes. Notice that as radio connectivity in Free Space increases and each node acquires complete network coverage, the number of link changes sinks toward zero.

Figure 6.11 shows us that indeed most of the disconnections in AF propagation are short-lived. We can see that most of the link breakages (as much as 88% with a sensitivity threshold of -91 dBm) last less than one second. As the sensitivity threshold increases, and connectivity

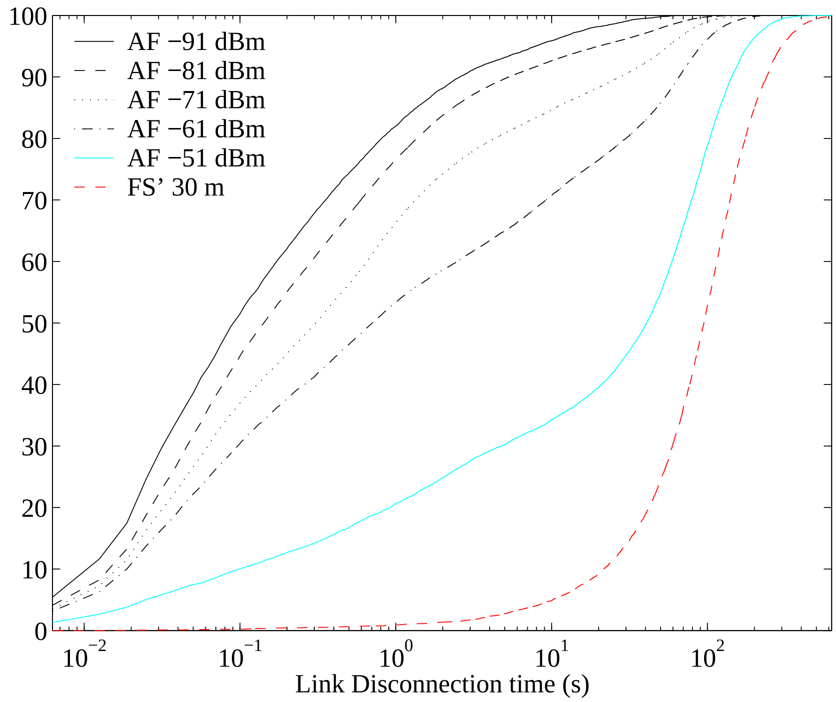

Figure 6.11: Cumulative Distribution of link disconnection times, for a network of 40 nodes with CM mobility and AF propagation. A typical FS′ configuration is offered for comparison.

consequently decreases, it is less likely for nodes to establish weaker links with faraway peers, more susceptible to experience these short disconnections. It is interesting to notice that the network size does not affect the distribution in the duration of link breakages; Figure 6.12 illustrates this.

The smooth and continuous characteristic of Free Space propagation results in a different behavior. Even though the duration of the link breakages under FS′ propagation is still affected by the transmission range, we can see in Figure 6.13 that the variation is significantly less pronounced than in AF propagation. Most importantly, the duration of the link breakages is longer than in AF propagation, as can be seen in Figures 6.11, 6.12 and 6.13. However, the massive difference in the total number of link breakages represents a significant factor in the protocols behavior.

For DSDV, more link breakages means more triggered updates. The CM-AF routing overhead curves in Figure 6.6 illustrate this. However, DSDV is not a reactive protocol, and hence

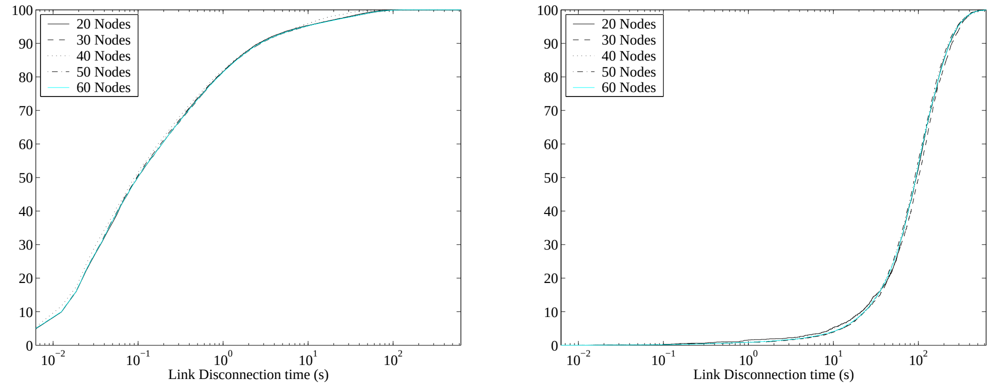

(a) AF propagation with a -91 dBm sensitivity threshold.

(b) FS′ propagation with a 30 m transmission range.

Figure 6.12: Link disconnection time CDFs, for CM mobility and networks of different sizes.

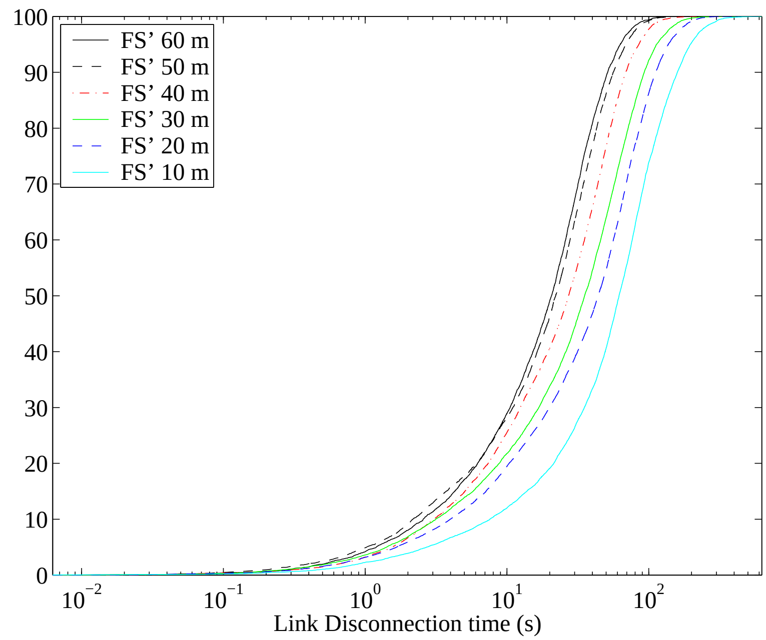

Figure 6.13: Link disconnection time CDFs, different transmission ranges for 40 nodes under FS′ propagation.

the degree of triggered update generation is controlled enough – review the timing constraints we listed in Table 2.2 – to prevent the protocol from collapsing. In general, DSDV is considered a sub-optimal protocol because it fails to converge in scenarios with rapid movement; in [7] it is reported to reach a roughly 70% PDR for nodes moving with a V_{max} of 20 m/s. However, while this lower performance is due to the intrinsic lack of quick adaptability of the protocol – a result of the same timing constraints that beneficially moderate its behavior in the scenarios we have considered – it is unlikely that node movement in indoor scenarios will reach such high speeds.

DSR is seriously affected by the much higher rate of link changes in CM-AF and CM-FS$'$. The protocol automatically reacts to any link breakage, short-lived or not. Route error packets are generated, and the cache is aggressively exploited to find alternative routes; with salvaging enabled, cache utilization will be substantially larger. However, the routes present in the cache offer no freshness guarantees: they may very well be stale routes, given the high number of link breakages occurring. Traffic is thus reinjected into the network using routes that may fail to deliver the packet; besides further occupying the scarcely available channel, the triggering of a potentially needed route discovery cycle is postponed. When the route discovery is finally started, the network is further clogged, leading to a congestion breakdown. As the number of nodes in the network increases, the higher number of link changes and neighboring nodes exacerbate the congestive effect.

In Table 6.1, we further explore the behavior of DSR by looking into three particular scenarios, with equivalent number of nodes and transmission power, but decreasing performance. We can identify a relationship between the increasing number of packet salvages and DSR's breakdown. We can also see that regardless of the situation, 90% or more of DSR's traffic is composed of unicast packets, much more costly than non-propagating broadcasts – the only type of routing packet in DSDV –, due to the RTS/CTS/DATA/ACK exchanges of the 802.11 DCF MAC protocol. Unicast packets that need to be forwarded along a multihop route are more susceptible to suffer multiple retransmissions in the hostile conditions we have de-

Experiment	RWP_S - FS′ 35 m range	CM - FS′ 35 m range	CM - AF -81 dBm threshold
PDR	99.96	42.61	11.24
Latency (ms)	43.33	11178	18608.39
Normalized Routing Load	17.81	484.62	5272.21
Routing Packets	27968.3	324167.8	929543.7
Route Request	1506.4 (5.39%)	29373.1 (9.09%)	87211.1 (9.38%)
Route Reply	23890.1 (85.41%)	251513.5 (77.58%)	689231.1 (74.15%)
Route Error	2571.3 (9.19%)	41316.2 (12.73%)	151025.2 (16.25%)
Unknown Flow Error	0.4 (0.01%)	1965 (0.6%)	2076.3 (0.22%)
Number of Packet Salvages	3509.2	114003.9	255055.4
Ratio of Salvaging per Packet	0.0224	0.7267	1.6258

Table 6.1: Detail of DSR routing activity for 50 nodes. For all experiments, 156875 application-layer packets are generated throughout the simulation.

scribed. Note that in scenarios with a bad performance, the number of route replies is extremely large; each retransmission is counted as one single transmission, since it occupies the wireless channel and prevents a rather large number of neighboring nodes from progressing in their activity. However, the 802.11 control exchanges for unicast packets are not completely effective in preventing collisions in scenarios with node mobility. Unfortunately, DSR assumes that any failure from the MAC layer to transmit a packet is due to a link breakage – even if the failure was caused by congestion, in the form of collisions or interference –, thus triggering the cycle of activity we have described, and further congesting the channel. This is a fine example of the care that must be taken for cross-layer interactions while designing a network protocol.

6.5 Discussion

While the CM-AF model is significantly more detailed than the simple models used in mainstream simulators (i.e. $\text{RWP}_\text{L}\text{-FS}'$), the model makes several simplifying assumptions, such as not modeling multiple floors or assuming a time-invariant channel, and therefore its robustness as a simplification of real-life conditions is not guaranteed.

Moreover, we conducted our experiments in a single indoor floorplan. Despite the complexity of such environment, both in terms of the layout and composition of its obstacles, it is not guaranteed that simplifying the simulation models in other indoor environments will have the same detrimental effects — or negligible effects for some cases, such as the 20 and 30 nodes experiments.

In this light, one should be careful not to view the results we present for DSDV and DSR as absolutely *realistic* predictors of the expected protocol performance in real-life indoor environments. Instead, in this thesis we consider the CM-AF results only as a benchmark against which to compare the simplified models. Given that the simplified models are not robust simplifications of CM-AF in our environment, we hypothesize that it is very unlikely that they are robust simplifications of real-world environments.

Following this hypothesis, we can also extract other interesting observations from the experimental results we have presented so far:

1. There is a drastic difference in the performance of DSR between CM-AF and CM-FS′, a strong indication that the sophistication of the radio propagation model can affect the results of the evaluation. The results obtained for LOS propagation further support this claim.

2. There are important differences in the delivery rate of DSR under CM-FS′ and Shell-FS′, which indicates that a sophisticated mobility model that contemplates internal walls – even without considering the effects these obstacles may have on radio propagation – can affect significantly the results of the evaluation.

3. It appears that Shell-FS$'$ and RWP_S-FS$'$ are equivalent models, since they yield practically the same performance in each experiment, and also present very similar values for each topology metric. We can conclude that once we have removed internal obstacles, both from the mobility and propagation models, external walls do not have a significant effect on the simulation results; it seems that the effective area of movement for the nodes becomes the only differentiating parameter.

Finally, we need to highlight the fact that while the effects that different simulation models have on the network topology – measured by the metrics we have presented in this thesis – are regular, intuitive and foreseeable, these sound characteristics do not necessarily translate into the performance trends of the routing protocols. Disregarding the two extreme cases – a lightly loaded network of 20 or 30 nodes and a completely overloaded network of 60 nodes in the DSR case –, we have verified that uniform topological trends translate into widely varying performance results, depending on the protocol used.

We have found that the internals of each protocol, and their interactions with other layers of the network stack, such as the MAC layer and presumably the transport layer, are complex and often surprising. In quantifying somehow these protocol dynamics, and devising a method to predict the effects of such dynamics on scenarios with uniform topological trends, lies a challenge that might render non-robust simplified simulation models usable as reliable trends illustrators.

Chapter 7

Related Work

In this Chapter we review related work in three areas:

- Improved mobility modeling.
- Realistic radio propagation models.
- Critical analyses of simulation models for MANET evaluation.

7.1 Mobility Modeling

Among the extensive literature on the RWP model, we highlight those efforts targeting the behavioral aspect of node mobility. Betstetter [28] and Camp et al. [12] reviewed several variations of RWP. In general, statistical distributions are employed to correlate the choice of new movement destinations or directions to past decisions. For instance, the Gauss-Markov Mobility Model [63] divides the simulation time into a fixed number of slices, and the speed and direction of a node in the n^{th} slice is highly dependent on the values chosen for the $n^{th} - 1$ slice. Another type of statistical behavioral modeling is presented in [64], in which exponential distributions are employed to influence the choice of node destinations.

A second family of node mobility models are those that model group behavior [65], also reviewed in [12, 66]. In a typical group mobility model, nodes are clustered into groups, and each group has a particular reference point. A node mobility model is used for each reference point, and a second mobility model governs the behavior of the associated nodes. Examples range from nodes orbiting randomly around the reference point, to nodes moving in an ordered line, or "chasing" the reference point.

A framework for systematically defining the behavior of a set of mobile nodes has been presented with the GEMM tool [13], which attempts to enable the modeling of node behavior after human activities. The tool therefore provides a set of constructs for designing behavioral models, including *attraction points*, *activities* and *roles*. It is worth pointing out that this work is at a very early stage, and it is not yet clear which of these constructs is useful, or usable.

Given that the emphasis of the CM model is placed on the modeling of physical obstacles, research on the behavioral aspects of node mobility is complementary to the work we have presented in this thesis. However, there is also a significant number of research papers devoted to the modeling of physical obstacles for mobility. Similar to CM, an enhanced mobility model uses some sort of graph to specify the physical constraints imposed on node movement. In general, these models target outdoor environments exclusively.

The City Section Mobility Model [67] uses a bi-dimensional grid to model vehicle movement on city streets in a coarse-grained manner. Node movement takes place between regularly spaced points in the grid, with the additional constraint that the translation from one grid intersection to another must involve at least one change of direction in each axis (dimension). Tian et al. [15] present a more flexible model in which an arbitrary user-defined graph, corresponding to the layout of the streets in a city, is used to restrict the movement of nodes. A third approach is presented by Jetcheva et al. [23], in which actual traces of city buses were used as the mobility pattern of nodes. Barring the natural transient offsets between the planned and actual schedules of a bus for a particular day, the novelty of this approach resides in its usage of a real-life mobility pattern, instead of presenting a model governed by a set of rules and random decisions.

The Obstacle Mobility Model (OM) [14] also provides modeling of physical obstacles, but at the smaller scale of building-to-building movement in a campus. OM uses automatically generated Voronoi graphs, based on the placement of rectangular boxes representing buildings – obstacles – in the modeled topography.

While many research groups have focused on outdoor environments, there is little work on indoor MANET simulation. Johansson et al. [8] considered conference, event coverage, and disaster area scenarios, with a few simple obstacles. Most of the nodes in the simulation are static or have little mobility, and only a few distinguished nodes move back and forth around predefined paths. Of the scenarios modeled, the conference room is the only indoors one.

Finally, the CAD-HOC [68] tool is presented as a "cousin" tool to the ns2 simulator for designing mobility patterns. Similar to the Obstacle Mobility model, CAD-HOC allows the arbitrary placement of obstacles in a topography; however, these obstacles can be sufficiently small to represent the layout of an indoor environment. Node mobility is only allowed in the areas with no obstacles, and the user can choose among a variety of random walk models for the nodes to move within these empty areas.

In general, there are two areas of physical mobility modeling in which little or no work has been carried out: the modeling of indoor environments, and the use of the original specification of an environment to model node mobility. Both of this issues are covered by our CM model, which models indoor environments based on their AutoCAD blueprints. The use of AutoCAD floor plans enables faithful modeling of fine-grained obstacles and significantly more complex indoor environments.

7.2 Radio Propagation Modeling

The literature on radio propagation models for wireless communication is abundant, dating back to the 1940's and 1950's, several years before the concept of MANETs. In general, radio propagation models are classified as indoor or outdoor models, and as deterministic or probabilistic models. Additionally, they are classified as models targeting the effects of large scale fading or those modeling small scale fading.

The AF model we employ in this thesis is derived from the original Attenuation Factor model proposed by Rappaport and Seidel [55, 56]; we have removed the Floor Attenuation Factor component, which allows consideration for multiple floors. A simpler variant of AF, called the Wall Attenuation Factor, was used in RADAR for location tracking [30]. In RADAR, the WAF model assumes a unique attenuation factor for all walls, and places an upper bound on the number of walls obstructing the primary ray that are taken into consideration. To the best of our knowledge, the AF model (or any variant of it) has never been used in MANET simulation prior to our work.

The AF model is an indoor deterministic model that in principle neglects the effects of multi-path propagation; it could be argued that since the model is derived from empirical measures, it integrates multipath effects into its parameters to a certain extent. A much more computationally expensive deterministic model that explicitly accounts for multipath fading effects is ray-tracing. Ray-tracing is based on the typical lighting algorithms employed in computer graphics, where a set of rays are cast from a light/radio source, and the multipath interactions of each ray with the environment – reflection, diffraction and scattering – are traced. Even though it is certainly more accurate than AF, the ray-tracing algorithm for a very simple indoor environment can be extremely time-consuming, even for a low number of rays cast and interactions considered. This complexity is the reason why ray-tracing implementations for MANET simulators [16] remain very limited in their scope.

In contrast to deterministic models, probabilistic propagation models simulate a homogeneous aggregate medium; stochastic methods are used to reproduce the variations in signal strength induced by obstacles. A very simple probabilistic augmentation to a deterministic model is Shadowing, which is provided by the ns2 [17] simulator, along with Two-Ray Ground and FS. The Shadowing model augments PL deterministic propagation with a zero-mean Gaussian random variable; the effect of this probabilistic component is an irregularity in the fringes of the coverage disc of a node.

Simulation of Indoor Radio Channel Impulse-Response Models (SIRCIM) [55, 69] is the most well-known example of probabilistic radio propagation modeling for indoor environments, simulating both large and small scale fading at the MAC and physical layers. Probabilistic distributions, such as Ricean and Rayleigh [70], are especially useful when modeling the effects of small scale fading; Ricean fading is employed for Line-Of-Sight conditions, while Rayleigh fading is employed in harsher non Line-Of-Sight situations. A good example on the use of Ricean and Rayleigh distributions in the scope of MANET simulations is the work by Takai et al. [71, 72]. Different researchers who have attempted experimental implementation of MANETs have shown that neglecting the effects of small scale fading is one of the most prejudicial simplifications of simulation [6, 5].

7.3 MANET Simulation Accuracy

Studies on simplified simulation models have focused on the limitations of either the mobility or the propagation model considered individually. Moreover, the potential effect that a simulation model enhancement may have in the evaluation of MANET routing protocols has been analyzed in a purely quantitative manner. In general, the papers cited in the previous sections of this chapter only report the numerical differences in performance between common simplified models and their new proposals.

We have been surprised by the scarcity of papers addressing the effects of simplified simulation models on the evaluation of MANETs in a qualitative manner. The relatively few studies of this kind usually focus on the effects of one model considered individually, and not on the combination of both mobility and radio propagation. A usually cited reference is the work by Heidemann et al. [73] on the characterization of the level of detail needed for different wireless simulation scenarios. This is a first indication of the lack of robustness of simplified simulation models: a simple propagation model is shown to be reliable enough for a certain scenario, but utterly inaccurate for a second distinct situation.

Lui et al. [11] gathered data from an experimental MANET deployment, and then compared the network performance to simulations with different radio propagation models, ranging from simple FS to Shadowing with Ricean and Rayleigh small scale fading. Their results show that "*the inaccuracy ... introduced by the propagation model is not-uniform and can undermine a performance comparison of different protocols*". However, this track is not explored in depth, as the authors are more concerned in showing the good properties of their simulation methodology; furthermore, only the need for validation of radio propagation models is addressed. We complement this result by showing that a well validated simplified simulation model is unreliable for any scenario different from that where the model was validated, even those with the minimal differences.

A result similar to that of Liu et al. was presented in [74], also for the case of radio propagation. However, this work was not so much a comparison of simulation models but of simulators themselves, in this case ns2 versus GloMoSim. Discrepancies between simulators have also been reported in [75], adding OpNet Modeler to the set of simulation tools under scrutiny. In general, the conclusions of the authors point to incomplete or inaccurate implementations of the 802.11 MAC and PHY layers as the main reason behind the observed inconsistencies.

These results complement ours in a troubling manner: they indicate that the MANET research community not only has to rethink the way their simulation models work, but also the way their simulation tools work. From a more general point of view, Pawlikowski et al. [76] also address the credibility problems of wireless simulation methodology. They review the increasing number of telecommunication networks simulation-based research papers, and assess the need for more rigorous simulation input generation and output data analysis.

To the best of our knowledge, we are the first group to consider detailed propagation and mobility models in conjunction, to focus on indoor environments, to identify robustness as a desirable property of simulation models, and to evaluate this qualitative property for commonly used simplified simulation models.

Chapter 8

Conclusions and future work

In this thesis we have addressed the robustness of simplifications of the mobility and radio propagation models for indoor simulation of MANET routing protocols. A simplification of a mobility or radio propagation model is robust if the results obtained with the simplification for different protocols and simulation conditions are within a consistent error of the expected result yielded by the unsimplified model. Robust simplifications allow researchers to extrapolate simulation results and reach reliable conclusions on the expected performance of real-life deployments.

We have developed two new detailed simulation models for indoor scenarios: Constrained Mobility and Attenuation Factor. Both models deterministically account for the presence of obstacles of different materials in the environment under consideration. Experimental results show that simplifications of these simulation model are not robust for (at least) indoor environments. The simplifications we considered had drastically different effects on the perceived performance of the two protocols we evaluated. Even for the same protocol, the effects on perceived performance varied erratically for different simulation configurations.

These results cast serious doubt on the validity of simulation-based MANET evaluations using simplified models. Even if a simplified model appears to be a good approximation for evaluating a specific MANET scenario, there are no assurances that the model will be valid for other routing protocols, or even the same protocol under different experimental conditions. This troubling conclusion is a compelling indication of the importance of further research on the development and validation of realistic models for indoor MANET simulation.

Addressing this sore need has become our preeminent future research goal. Even though detailed models such as those presented in this thesis, CM and AF, are more accurate alternatives for MANET simulation and will likely yield more reliable results, it is also true that these models require a significantly larger implementation effort and impose longer simulation run times. In order to minimize user effort and maximize time efficiency, we need to investigate under which conditions can simplified models be used and still yield acceptable results. For example, there does not seem to be any significant difference between the results obtained with $\mathrm{RWP_L}$-FS′ and CM-AF for the DSDV routing protocol; however, translating such assumption to the use of DSR would be a gross mistake. It therefore becomes instrumental to devise a method that identifies the minimum level of simulation detail required to obtain reliable results for a given experimental scenario.

Our plans for future work span three other directions. We will concentrate our efforts on further validating the results we have obtained, by applying the same methodology to other indoor scenarios. We will carefully choose indoor floor plans that offer a variety of challenges departing from those presented by the Bahen Centre. We plan to work with even more complex scenarios, with modern and intricate architectural designs, but also to consider simpler scenarios with a more regular layout.

Our third goal for future research is to enhance the simulation models we have presented. Both models currently do not take into account smaller obstacles such as furniture, or the presence of other people. Also, for Constrained Mobility, we plan to complement the model with one of the behavioral modeling proposals we have found in the literature. For Attenuation Factor, we want to add a small scale fading component – most likely by adding Ricean and Rayleigh fading distributions, which are already available for the ns2 simulator –, as it has been thoroughly shown that assuming a time-invariant channel leads to incomplete results and erroneous design decisions in routing protocol development.

Finally, our fourth future work goal entails the extension of the simulation models to consider three-dimensional floor plans. This goal can be attained through addition of a third coordinate to the CM mobility graph's vertices, and by reinserting the Floor Attenuation Factor component to the AF model. Validation of a three-dimensional propagation model will be, however, a much more complex and certainly rewarding task.

Appendix

Empirical Signal Strength Measurements

We present the empirical data gathered from our signal strength measurements. Figure A.1 depicts the Bahen's fifth floor, with the subset of the mobility graph employed to obtain the random locations for measurements. The parts of the mobility graph that were cropped out represent offices to which we could not obtain access. Notice that each vertex in the graph is numbered to facilitate the usage of Table A.1, where the measurements performed are listed. For each measurement we provide the pair of locations involved, the distance between those two locations, the average signal strength recorded, and the number of primary-ray obstructing walls for each of the four combinations of materials we considered.

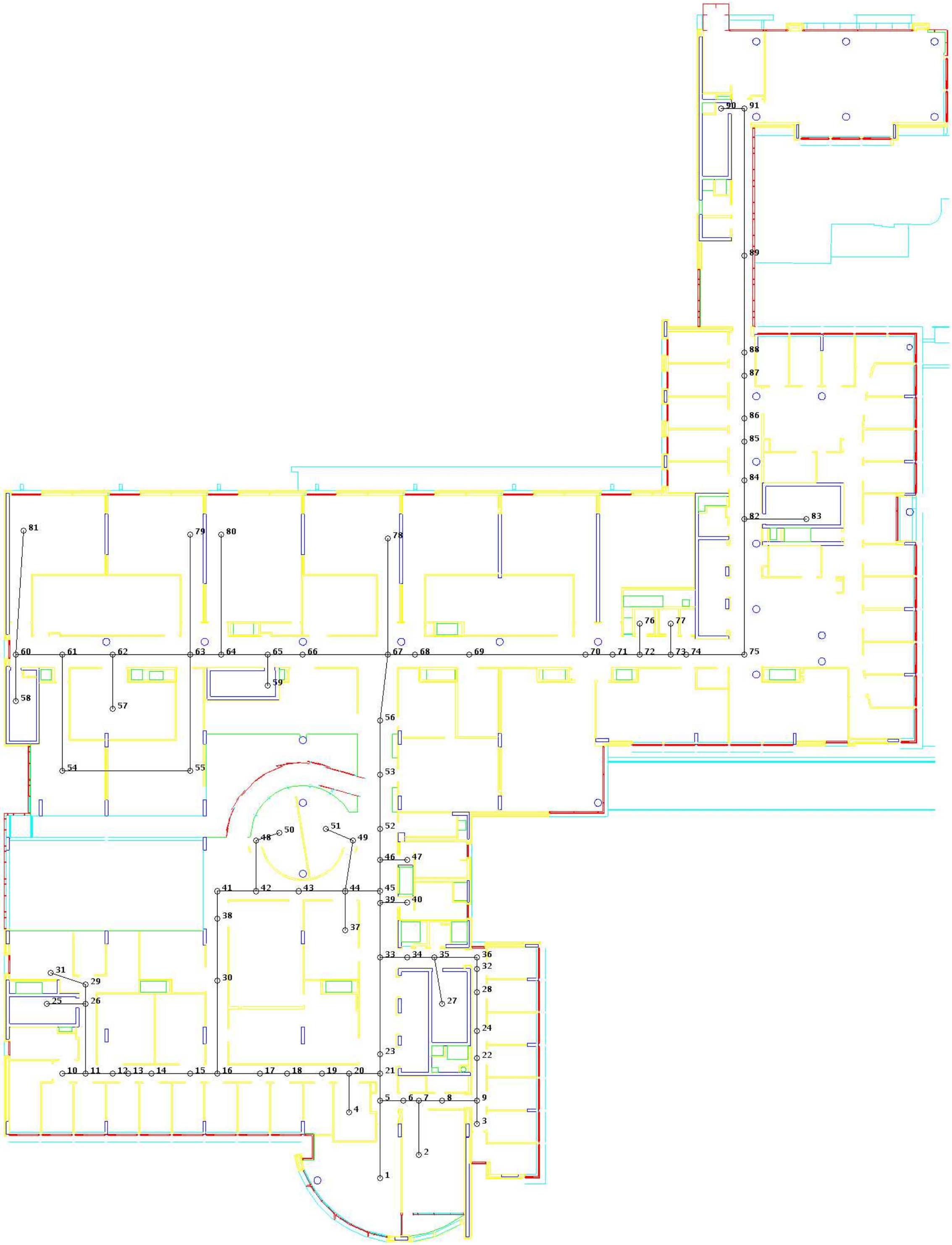

Figure A.1: Subset of the CM mobility graph employed to obtain the measurement locations, superimposed on the Bahen's fifth floor blueprint.

A	B	Distance(m)	Signal Strength (dBm)	steel/cement	drywall/wood	glass	brick
80	59	14.435892000	-100.050003000	1	2	0	0
80	16	49.085700000	-98.883331500	2	1	1	0
80	68	21.095390000	-78.283333000	1	2	0	0
80	40	37.750232000	-89.366669000	1	5	2	0
80	35	43.301244000	-93.650001500	1	7	2	0
80	47	34.344593000	-92.483330000	0	4	2	0
80	48	28.085076000	-83.783340000	2	2	3	0
80	90	60.608369000	-108.500000000	1	1	0	2
80	65	11.771343000	-62.250000000	0	2	0	0
80	55	21.732997000	-75.849998500	1	2	0	0
82	11	79.429411000	-112.000000000	4	19	2	0
82	91	37.431250000	-64.599998500	0	0	0	0
82	88	15.184375000	-55.816665500	0	0	0	0
82	67	35.407461000	-99.016662500	2	5	0	0
82	36	47.026959000	-113.000000000	3	5	3	2
82	69	28.433254000	-95.983337000	4	4	0	0
82	86	9.181250000	-47.733329500	0	0	0	0
82	83	5.770492000	-72.416664000	1	0	0	0
82	56	38.555188000	-101.750000000	3	8	0	0
84	60	69.640481000	-95.750000000	3	6	0	1
84	68	34.529498000	-87.766670000	3	6	0	0
84	82	3.531250000	-50.799995500	0	0	0	0
84	75	15.890625000	-62.216667500	0	0	0	0
84	47	46.713079000	-111.500000000	3	12	0	0
84	70	21.706311000	-82.433334000	3	7	0	0
84	87	9.534375000	-46.683334000	0	0	0	0
83	91	37.873435000	-99.466667000	1	2	2	0
90	84	33.968995000	-105.333335500	2	3	0	0
90	91	2.163934000	-76.766663000	1	0	0	0
90	89	13.592110000	-87.950004500	1	1	0	0
90	88	22.351869000	-96.649994000	1	2	0	0
90	87	24.461527000	-97.783333000	1	2	0	0
77	72	4.037978000	-53.099998500	0	1	0	0
77	67	26.478997000	-82.483330000	1	6	0	0
77	47	32.641294000	-109.966667000	1	9	0	0
77	63	44.810449000	-86.283333000	1	6	0	0
77	86	19.930650000	-88.566666000	3	6	0	0
77	85	17.955847000	-92.099998500	3	6	0	0
77	75	7.411938000	-64.849998500	2	2	0	0
88	76	26.567640000	-95.783332500	0	5	0	1
88	67	43.122991000	-99.183334000	2	4	1	2

Table A.1: Empirical Signal Strength Measurements.

A	B	Distance(m)	Signal Strength (dBm)	steel/cement	drywall/wood	glass	brick
88	76	26.567640000	-95.783332500	0	5	0	1
88	91	22.246875000	-52.666664000	0	0	0	0
88	71	30.149992000	-83.099998500	0	7	0	1
88	84	11.653125000	-61.516662500	0	0	0	0
88	87	2.118750000	-37.550003000	0	0	0	0
48	39	12.849778000	-58.483337000	0	2	0	0
48	12	25.039559000	-76.033333000	0	6	2	0
48	75	48.500871000	-99.516670000	1	6	1	0
48	36	23.126463000	-84.049995500	1	7	0	0
48	38	7.930080000	-51.266670500	0	2	0	0
48	73	42.148585000	-97.883331500	0	7	1	0
48	28	24.744096000	-92.683334500	4	8	0	0
48	72	39.523963000	-96.000000000	0	6	1	0
85	71	22.968960000	-84.133331500	2	8	0	0
85	64	52.419287000	-90.449997000	2	7	2	0
85	67	38.446630000	-95.699997000	2	6	0	1
85	53	45.514636000	-108.450004500	1	8	0	1
85	82	7.062500000	-45.166671500	0	0	0	0
85	69	32.138840000	-94.266670500	1	4	0	1
85	91	30.368750000	-60.000000000	0	0	0	0
85	89	16.950000000	-55.483337500	0	0	0	0
85	84	3.531250000	-40.333336000	0	0	0	0
10	64	40.903800000	-101.683334500	3	6	3	0
10	16	14.426230000	-50.516662500	0	0	0	0
10	15	11.901639000	-47.516670000	0	0	0	0
10	44	31.122547000	-89.900001500	0	7	0	0
10	69	53.744943000	-107.616661000	1	11	4	0
10	18	20.918033000	-52.716667000	0	0	0	0
10	19	24.163934000	-57.116668500	0	0	0	0
10	3	38.862251000	-95.483337000	0	10	0	0
10	65	42.659615000	-105.716667000	2	5	4	0
39	56	16.596875000	-53.266662500	0	0	0	0
39	32	10.832029000	-66.699997000	1	5	0	0
39	74	36.366782000	-97.866661500	2	6	0	2
39	10	33.406913000	-76.866668500	1	5	0	0
39	13	28.124197000	-82.966667000	0	6	0	0
39	45	1.059375000	-42.183334000	0	0	0	0
16	28	25.276218000	-97.133331500	3	4	0	0
16	74	57.955684000	-104.766670000	0	12	1	1
16	12	9.737705000	-46.399994000	0	0	0	0
16	33	18.484467000	-71.766662500	0	4	0	0

Table A.1: Empirical Signal Strength Measurements (cont.).

A	B	Distance(m)	Signal Strength (dBm)	steel/cement	drywall/wood	glass	brick
16	42	16.984214000	-62.866661000	0	3	0	0
16	70	51.267668000	-93.333335500	1	12	0	0
16	58	38.741789000	-105.916671500	1	6	3	0
16	54	31.092994000	-79.366661000	0	3	3	0
16	15	2.524590000	-35.316665500	0	0	0	0
16	60	42.499237000	-94.983330000	3	6	3	0
13	53	35.901068000	-82.083335500	0	8	1	0
13	55	28.141726000	-78.500000000	0	3	3	0
13	25	9.887564000	-60.466667000	1	3	0	0
13	23	23.509020000	-78.133331000	0	2	0	0
13	14	2.163934000	-37.816673000	0	0	0	0
13	69	49.616034000	-99.166664000	1	11	1	0
13	18	14.786885000	-47.949997000	0	0	0	0
13	63	38.571589000	-89.916671500	0	4	3	0
13	65	40.287007000	-101.783332500	3	3	2	0
54	19	36.640877000	-88.466667500	1	3	3	0
54	65	21.854093000	-76.433334500	3	3	0	0
54	63	15.933504000	-67.116668500	0	2	1	0
54	16	31.092994000	-79.366661000	0	3	3	0
54	55	11.901639000	-48.966667000	0	1	0	0
54	57	7.341986000	-51.599998500	0	0	1	0
54	72	54.771968000	-86.116668500	1	6	1	0
54	68	34.487076000	-80.300003000	1	4	0	0
54	30	23.910946000	-63.966660000	0	1	3	0
54	75	64.353362000	-92.950004500	0	8	2	0
53	52	4.943750000	-41.466667000	0	0	0	0
53	72	26.527906000	-87.599998500	0	4	0	0
53	38	20.003963000	-63.516662500	0	4	1	0
53	81	39.948187000	-86.233330000	2	2	1	0
53	18	28.535099000	-75.616669000	1	4	1	0
53	82	41.140035000	-109.599998500	3	10	0	0
53	59	13.242201000	-83.183334500	1	0	1	0
53	14	34.526985000	-75.533333000	1	6	1	0
53	57	25.599081000	-78.150001500	1	2	1	0
60	61	4.327869000	-44.683334500	0	0	0	0
60	62	9.016393000	-52.400001500	0	0	0	0
60	63	16.229508000	-47.333336000	0	0	0	0
60	65	23.442623000	-58.449997000	0	0	0	0
60	66	26.688525000	-55.433334500	0	0	0	0
60	67	34.622951000	-62.783333000	0	0	0	0
60	69	42.196721000	-62.550003000	0	0	0	0

Table A.1: Empirical Signal Strength Measurements (cont.).

A	B	Distance(m)	Signal Strength (dBm)	steel/cement	drywall/wood	glass	brick
60	70	53.016393000	-63.850006000	0	0	0	0
60	72	58.065574000	-61.983329500	0	0	0	0
60	75	67.803279000	-67.450004500	0	0	0	0
62	8	50.881191000	-106.099998500	2	13	3	0
62	31	29.525633000	-79.083335500	0	1	4	0
62	63	7.213115000	-47.716660000	0	0	0	0
62	45	32.913128000	-85.400001500	1	5	2	0
62	81	14.017788000	-64.616668500	1	2	0	0
62	15	38.813631000	-81.433334500	0	4	3	0
62	58	9.962518000	-78.800003000	1	4	0	0
62	41	23.639404000	-74.466667500	0	2	3	0
62	5	47.627689000	-90.033333000	1	9	0	0
62	69	33.180328000	-62.199997000	0	0	0	0
41	44	11.901639000	-50.966667000	0	0	0	0
41	59	19.293960000	-95.133339000	1	0	3	0
41	62	23.639404000	-74.466667500	0	2	3	0
41	17	17.064438000	-95.100006000	0	3	0	0
41	50	7.832973000	-50.450004500	0	1	0	0
41	38	2.471875000	-40.650001500	0	0	0	0
4	75	55.583807000	-105.633331000	3	7	1	2
4	33	14.416666000	-57.433334000	0	2	0	0
4	6	5.159118000	-60.650001500	0	1	0	0
4	38	21.496675000	-73.616661000	1	5	0	0
4	50	26.240696000	-76.883331500	1	5	1	0
4	25	29.818184000	-108.416664000	1	6	0	0
4	19	4.340885000	-45.133331500	0	2	0	0
4	3	11.948694000	-64.500000000	0	3	0	0
4	59	39.575231000	-109.233330000	2	6	3	0
4	10	26.921127000	-66.366661000	0	7	0	0
44	55	18.109395000	-68.616669000	0	3	2	0
44	31	28.395257000	-75.266663000	1	6	1	0
44	32	14.150717000	-73.199997000	1	3	0	0
44	78	32.378339000	-62.533333000	0	3	2	0
44	65	22.716240000	-74.416671500	2	1	3	0
44	76	36.674007000	-105.949997000	1	6	0	0
44	42	8.295082000	-56.216667000	0	0	0	0
44	38	12.155624000	-64.883331000	0	2	1	0
6	39	18.138914000	-68.616669000	2	4	0	0
6	63	45.195031000	-96.449997000	1	8	3	0
6	7	1.442623000	-39.883338500	0	0	0	0
6	48	27.342107000	-88.266663000	0	9	1	0

Table A.1: Empirical Signal Strength Measurements (cont.).

A	B	Distance(m)	Signal Strength (dBm)	steel/cement	drywall/wood	glass	brick
6	13	25.725589000	-70.933334500	0	5	0	0
6	28	12.029915000	-70.533333000	4	4	0	0
6	3	7.172538000	-68.616669000	0	2	0	0
6	74	48.397087000	-107.183327000	4	7	2	2
42	61	28.092346000	-72.399994000	0	2	1	0
42	18	16.845798000	-64.783332500	0	3	0	0
42	65	21.567781000	-79.966667500	2	1	3	0
42	43	3.967213000	-40.849998500	0	0	0	0
42	67	24.786335000	-77.366669000	1	3	3	0
42	71	39.559230000	-100.333328500	1	7	1	0
42	78	34.394504000	-76.516663000	0	4	3	0
1	5	7.062500000	-56.083328500	0	1	0	0
1	21	9.534375000	-54.799995500	0	1	0	0
1	23	11.300000000	-53.933334500	0	1	0	0
1	33	20.128125000	-61.500000000	0	1	0	0
1	39	25.071875000	-68.916664000	0	1	0	0
1	45	26.131250000	-63.566666000	0	1	0	0
1	46	28.956250000	-62.750000000	0	1	0	0
1	52	31.781250000	-60.083336000	0	1	0	0
1	53	36.725000000	-64.716667000	0	1	0	0
1	56	41.668750000	-70.266662500	0	1	0	0
1	56	41.668750000	-70.266662500	0	1	0	0
73	42	44.195014000	-99.466667000	1	8	1	0
73	89	37.011748000	-95.316665500	2	10	0	0
73	75	6.852459000	-45.516670500	0	0	0	0
73	68	23.803279000	-56.750000000	0	0	0	0
73	36	32.921719000	-109.766663000	0	2	3	2
73	53	29.180340000	-88.116668500	0	7	0	0
73	84	17.305148000	-70.250000000	2	3	0	0
73	62	51.934426000	-61.316666000	0	0	0	0
73	40	33.349895000	-102.583336000	1	7	1	2
73	69	18.754098000	-58.183334500	0	0	0	0
54	15	30.005119000	-81.033333000	0	4	3	0
54	26	21.297717000	-64.599998500	0	1	3	0
54	58	7.689757000	-74.150001500	1	1	0	0
54	18	34.586446000	-82.583336000	0	4	3	0
54	61	10.593750000	-46.949997000	0	1	0	0
54	59	20.633160000	-92.433334000	1	3	0	0
54	38	19.702257000	-68.866668500	1	0	3	0
56	65	12.059375000	-51.133331000	0	2	0	0
56	70	20.035252000	-71.833336000	0	4	0	0

Table A.1: Empirical Signal Strength Measurements (cont.).

A	B	Distance(m)	Signal Strength (dBm)	steel/cement	drywall/wood	glass	brick
56	57	24.907785000	-63.250000000	0	2	1	0
56	11	42.236444000	-80.900001500	1	6	3	0
56	74	29.117355000	-73.683334500	0	6	0	0
56	69	10.239428000	-64.416664500	0	3	0	0
56	75	34.429038000	-76.449997000	0	7	0	0
57	34	35.525471000	-89.500000000	0	7	3	0
57	55	9.162506000	-51.016662500	0	1	0	0
57	67	26.079426000	-70.566665500	2	4	0	0
57	59	14.580988000	-86.283332500	1	2	0	0
57	61	6.813437000	-56.699997000	0	1	0	0
57	41	19.242639000	-61.883331500	0	1	3	0
57	39	30.512598000	-77.883331000	0	4	2	0
57	23	40.087436000	-84.283333000	0	6	1	0
57	76	49.660604000	-108.016663000	3	8	0	0
79	46	34.527788000	-90.416664000	3	2	5	0
79	62	13.109657000	-52.316666000	0	2	0	0
79	67	21.404504000	-72.466667000	1	2	0	0
79	56	24.486868000	-80.416664500	2	4	0	0
79	59	15.546497000	-99.099998500	2	2	0	0
79	70	38.381102000	-87.866669000	1	6	0	0
79	32	47.712471000	-108.716667000	4	12	2	0
79	16	49.149257000	-84.733337000	2	2	2	0
24	46	17.964110000	-87.700004500	3	5	0	0
24	66	37.903476000	-104.183334500	3	8	2	0
24	52	20.456704000	-87.950004500	4	9	0	0
24	69	34.260719000	-102.383331500	0	3	1	1
24	20	12.519480000	-74.500000000	3	1	0	0
24	35	7.794517000	-61.050003000	2	1	0	0
24	22	2.471875000	-38.250000000	0	0	0	0
24	53	24.989531000	-87.766670500	3	9	0	0
34	24	9.335910000	-63.566665500	3	2	0	0
34	40	4.943750000	-64.083335500	0	2	0	0
34	65	30.450488000	-73.900001500	3	4	3	0
34	54	36.298860000	-75.333335500	1	3	3	0
34	35	2.524590000	-53.766670000	0	0	0	0
34	55	26.366836000	-68.099998500	0	6	2	0
34	41	18.663915000	-71.949997000	0	3	0	0
34	71	33.526586000	-85.899994000	0	9	0	2

Table A.1: Empirical Signal Strength Measurements (final).

Bibliography

[1] D. B. Johnson and D. A. Maltz, “Dynamic source routing in ad hoc wireless networks,” in *Mobile Computing*, Imielinski and Korth, Eds. Kluwer Academic Publishers, 1996, vol. 353.

[2] C. Perkins and P. Bhagwat, “Highly dynamic destination-sequenced distance-vector routing (DSDV) for mobile computers,” in *Proceedings of ACM SIGCOMM’94 – Conference on Communications Architectures, Protocols and Applications*, London, UK, Aug. - Sept. 1994, pp. 234–244.

[3] C. E. Perkins and E. M. Royer, “Ad hoc on demand distance vector routing,” in *Proceedings of WMCSA ’99 – 2nd IEEE Workshop on Mobile Computing Systems and Applications*, New Orleans, LA, Feb. 1999, pp. 90–100.

[4] C. Tschudin, H. Lundgren, and E. Nordstrom, “Embedding MANETs in the real world,” in *Proceedings of PWC ’03 – Personal Wireless Communications*, Venice, Italy, Sep 2003.

[5] D. A. Maltz, J. Broch, and D. B. Johnson, “Quantitative lessons from a full-scale multi-hop wireless ad hoc network testbed,” in *Proceedings of WCNC 2000 – IEEE Wireless Communications and Networking Conference*, vol. 3, Chicago, IL, Sept. 2000, pp. 992 – 997.

[6] K.-W. Chin, J. Judge, A. Williams, and R. Kermode, “Implementation experience with manet routing protocols,” *ACM SIGCOMM Computer Communications Review*, pp. 45–49, Nov. 2002.

[7] J. Broch, D. A. Maltz, D. B. Johnson, Y.-C. Hu, and J. Jetcheva, “A performance comparison of multi-hop wireless ad hoc network routing protocols,” in *Proceedings of MobiCom ’98 – Fourth Annual International Conference on Mobile Computing and Networking*, Dallas, TX, Oct. 1998, pp. 85–97.

[8] P. Johansson, T. Larsson, N. Hedman, B. Mileczarek, and M. Degermark, “Scenario-based performance analysis of routing protocols for mobile ad-hoc networks,” in *Proceedings of MobiCom ’99 – 5th annual ACM/IEEE international conference on Mobile Computing and Networking*, Seattle, WA, Aug. 1999, pp. 195–206.

[9] S. R. Das, C. E. Perkins, and E. E. Royer, “Performance comparison of two on-demand routing protocols for ad hoc networks,” in *Proceedings of INFOCOM ’00 – IEEE Conference on Computer Communications*, vol. 1, Tel-Aviv, Israel, Mar. 2000, pp. 3–12.

[10] H.-Y. H. Hsieh and R. Sivakumar, “On using peer-to-peer communication in cellular wireless data networks,” *IEEE Transactions on Mobile Computing*, vol. 3, no. 1, pp. 57–72, Jan. 2004.

[11] J. Liu, Y. Yuan, D. M. Nicol, R. S. Gray, C. C. Newport, D. Kotz, and L. F. Perrone, “Simulation validation using direct execution of wireless ad-hoc routing protocols,” in *Proceedings of PADS – Workshop on Parallel and Distributed Simulation*, Kufstein, Austria, May 2004, pp. 7–16.

[12] T. Camp, J. Boleng, and V. Davies, “A survey of mobility models for ad hoc network research,” *Wireless Communications & Mobile Computing (WCMC): Special issue on Mobile Ad Hoc Networking: Research, Trends and Applications*, vol. 2, no. 5, pp. 483–502, 2002.

[13] S. Ray, “Realistic mobility for manet simulation,” Master’s thesis, University of British Columbia, 2003.

[14] A. Jardosh, E. M. Belding-Royer, K. C. Almeroth, and S. Suri, "Towards realistic mobility models for mobile ad hoc networks," in *Proceedings of MobiCom '03 – Ninth Annual International Conference on Mobile Computing and Networking*, San Diego, CA, Sept. 2003, pp. 217–229.

[15] J. Tian, J. Hahner, C. Becker, I. Stepanov, and K. Rothermel, "Graph-based mobility model for mobile ad hoc network simulation," in *Proceedings of the 35th Annual Simulation Symposium*, San Diego, USA, Apr. 2002, pp. 337–344.

[16] J.-M. Dricot and P. D. Doncker, "High accuracy physical layer models for wireless network simulations in ns-2," in *Proceedings of IWAN '04 – International Workshop on Wireless Ad-hoc Networks*, Oulu, Finland, May–June 2003.

[17] N. Drakos and R. Moore, *ns2 - The Manual (formerly Notes and Documentation)*, 1999. [Online]. Available: http://www.isi.edu/nsnam/ns/doc/

[18] The Monarch Project. [Online]. Available: http://www.monarch.cs.rice.edu

[19] T. Larsson and N. Hedman, "Routing protocols in wireless ad-hoc networks–a simulation study." Master's thesis, Lulea University of Technology, 1998.

[20] A. Hamidian, "A study of internet connectivity for mobile ad hoc networks in ns 2." Master's thesis, Lund Institute of Technology, 2003.

[21] Y.-C. Hu and D. B. Johnson, "Exploiting congestion information in network and higher layer protocols in multihop wireless ad hoc networks," in *Proceedings of ICDCS '04 – 24th IEEE International Conference on Distributed Computing Systems*, Tokyo, Japan, Mar. 2004, pp. 301–310.

[22] Y.-C. Hu, A. Perrig, and D. B. Johnson, "Ariadne: A secure on-demand routing protocol for ad hoc networks," in *Proceedings of MobiCom '02 – Eighth Annual International Conference on Mobile Computing and Networking*, Atlanta, GA, Sept. 2002, pp. 12–23.

[23] J. G. Jetcheva, Y.-C. Hu, S. PalChaudhuri, A. K. Saha, and D. B. Johnson, "Design and evaluation of a metropolitan area multitier wireless ad hoc network architecture," in *Proceedings of WMCSA '03 – 5th IEEE Workshop on Mobile Computing Systems and Applications*, Monterey, CA, Oct. 2003, pp. 9–10.

[24] T. Camp, J. Boleng, B. Williams, L. Wilcox, and W. Navidi, "Performance comparison of two location based routing protocols for ad hoc networks," in *Proceedings of INFOCOM '02 – IEEE Conference on Computer Communications*, vol. 3, New York, NY, June 2002, pp. 1678–1687.

[25] L. Bajaj, M. Takai, R. Ahuja, R. Bagrodia, and M. Gerla, "Glomosim: A scalable network simulation environment," University of California, Los Angeles, Tech. Rep. 990027, 1999.

[26] OpNet network modeler. [Online]. Available: http://www.opnet.com

[27] J. Yoon, M. Liu, and B. Noble, "Random waypoint considered harmful," in *Proceedings of INFOCOM '03 – IEEE Conference on Computer Communications*, vol. 2, San Francisco, CA, May–Apr. 2003, pp. 1312–1321.

[28] C. Bettstetter, "Mobility modeling in wireless networks: categorization, smooth movement, and border effects," *ACM SIGMOBILE Mobile Computing and Communications Review*, vol. 5, no. 3, pp. 55–66, July 2001.

[29] H. H. Xia, "Radio propagation characteristics for line-of-sight microcellular and personal communication," *IEEE Transactions on Antennas and Propagation*, vol. 41, no. 10, pp. 1439–1447, Oct. 1993.

[30] P. Bahl and V. N. Padmanabhan, "RADAR: An in-building RF-based user location and tracking system," in *Proceedings of INFOCOM '00 – IEEE Conference on Computer Communications*, vol. 2, Tel-Aviv, Israel, Mar. 2000, pp. 775–784.

[31] B. Sklar, “Rayleigh fading channels in mobile digital communication systems part I and II: Characterization and Mitigation,” *IEEE Communications Magazine*, vol. 35, no. 9, pp. 136–155, Sept. 1997.

[32] L. Kleinrock and F. A. Tobagi, “Packet switching in radio channels: Part I - carrier sense multiple-access modes and their throughput-delay characteristics,” *IEEE Transactions on Communications*, vol. 23, pp. 1417–1433, Dec. 1975.

[33] P. Karn, “MACA - A new channel access protocol for packet radio,” in *Proceedings of the ARRL/CRRL Amateur Radio Ninth Computer Networking Conference*, 1990, pp. 134–140.

[34] C. L. Fullmer and J. J. Garcia-Luna-Aceves, “Floor acquisition multiple access (FAMA) for packet-radio networks,” in *Proceedings of the Conference on Applications, technologies, architectures, and protocols for computer communication*, Cambridge, MA, 1995, pp. 262–273.

[35] *Wireless LAN Medium Access Control and Physical Layer Specification*, The IEEE Computer Society LAN and MAN Standards Committee, Aug. 1999, 802.11 Standard.

[36] E. M. Royer, S.-J. Lee, and C. E. Perkins, “The effects of MAC protocols on ad hoc network communication,” in *Proceedings of WCNC 2000 – IEEE Wireless Communications and Networking Conference*, vol. 2, Chicago, IL, Sept. 2000, pp. 543–548.

[37] S. J. Lee, “Routing and multicasting strategies in wireless mobile ad hoc networks,” Ph.D. dissertation, University of California, Los Angeles, 2000.

[38] D. B. Johnson, D. A. Maltz, and J. Broch, “DSR: The dynamic source routing protocol for multi-hop wireless ad hoc networks,” in *In Ad Hoc Networking*, C. Perkins, Ed. Addison Wesley, 2001, pp. 139–172.

[39] J. Macker and S. Corson. Mobile Ad-hoc Networks (manet) IETF charter. [Online]. Available: http://www.ietf.org/html.charters/manet-charter.html

[40] C. Perkins, E. Belding-Royer, S. Das, and I. Chakeres. Ad hoc on-demand distance vector routing. [Online]. Available: http://moment.cs.ucsb.edu/AODV/aodv.html#Implementations

[41] V. D. Park and M. S. Corson, "A highly adaptive distributed routing algorithm for mobile wireless networks," in *Proceedings of INFOCOM '97 – IEEE Conference on Computer Communications*, vol. 3, Kobe, Japan, Apr. 1997, pp. 1405–1413.

[42] C.-K. Toh, "Associativity-based routing for ad hoc mobile networks," *Wireless Personal Communications*, vol. 4, no. 2, pp. 103–139, 1997.

[43] S. Murthy and J. J. Garcia-Luna-Aceves, "An efficient routing protocol for wireless networks," *Mobile Networks and Applications*, vol. 1, no. 2, pp. 183–197, 1996.

[44] W. L. C. Chiang, H. Wu and M. Gerla, "Routing in clustered multihop, mobile wireless networks," in *Proceedings of IEEE SICON '97 – Singapore International Conference on Networks*, Singapore, Apr. 1997, pp. 197–211.

[45] T. Clausen, P. Jacquet, A. Laouiti, P. Muhlethaler, and L. Qayyum, A. andViennot, "Optimized link state routing protocol," in *Proceedings of IEEE INMIC – Multi Topic Conference*, Pakistan, Dec. 2001, pp. 62–68.

[46] Z. J. Haas and M. R. Pearlman, "The zone routing protocol (ZRP) for ad hoc networks," IETF Internet Draft, draft-ietf-manet-zone-zrp-04.txt, July 2002.

[47] Y.-B. Ko and N. H. Vaidya, "Location-aided routing (LAR) in mobile ad hoc networks," *Wireless Networking*, vol. 6, no. 4, pp. 307–321, 2000.

[48] S. Basagni, I. Chlamtac, V. R. Syrotiuk, and B. A. Woodward, "A distance routing effect algorithm for mobility (DREAM)," in *Proceedings of MobiCom '98 – Fourth Annual*

International Conference on Mobile Computing and Networking, Dallas, TX, Oct. 1998, pp. 76–84.

[49] R. Jain, A. Puri, and R. Sengupta, “Geographical routing using partial information for wireless ad hoc networks,” University of California, Berkeley, Tech. Rep. M99/69, Dec. 1999.

[50] E. M. Royer and C. K. Toh, “A review of current routing protocols for ad hoc mobile wireless networks,” *IEEE Personal Communications*, vol. 6, no. 2, pp. 46–55, Apr. 1999.

[51] F. Baker. An outsider’s view of MANET. Draf-baker-manet-review-01. [Online]. Available: http://w3.antd.nist.gov/wctg/manet/draft-baker-manet-review-01.txt

[52] Y.-C. Hu and D. B. Johnson, “Implicit source routing in on-demand ad hoc network routing,” in *Proceedings of MobiHoc ’01 – Second ACM Symposium on Mobile Ad Hoc Networking and Computing*, Long Beach, CA, Oct. 2001, pp. 1–10.

[53] T. H. Cormen, C. E. Leiserson, and R. L. Rivest, *Introduction to Algorithms*. MIT Press, 1990.

[54] Open Design Alliance. [Online]. Available: http://www.opendwg.org

[55] T. S. Rappaport, *Wireless Communications: Principles & Practice*. Prentice Hall, 2002.

[56] S. Y. Seidel and T. S. Rappaport, “Site-specific propagation prediction for wireless in-building personal communication system design,” *IEEE Transactions on Vehicular Technology*, vol. 43, no. 4, pp. 879–891, Apr. 1994.

[57] J. Tourrilhes. Wireless Tools for Linux. [Online]. Available: http://www.hpl.hp.com/personal/Jean%5fTourrilhes/Linux/Tools.html

[58] Enterasys RoamAbout wireless high-rate pc card. [Online]. Available: http://www.enterasys.com/products/wireless/CSIxD-AA/

[59] Superpass SPDG80-D3 antenna specifications sheet. [Online]. Available: http://www.superpass.com/SPDG8O-D3.html

[60] C. S. Balanis, *Advanced Engineering Electromagnetics*. Wiley Text Books, 1989.

[61] T. A. Elbatt, S. V. Krishnamurthy, D. Connors, and S. Dao, "Power management for throughput enhancement in wireless ad hoc networks," in *Proceedings of ICC '00 – IEEE International Conference on Communications*, New Orleans, LA, June 2000, pp. 1503–1513.

[62] R. Ramanathan and R. Rosales-Hain, "Topology control of multihop wireless networks using transmit power adjustment," in *Proceedings of INFOCOM '00 – IEEE Conference on Computer Communications*, vol. 2, Tel-Aviv, Israel, Mar. 2000, pp. 404–413.

[63] V. Tolety, "Load reductions in ad hoc networks using mobile servers," Master's thesis, Colorado School of Mines, 1999.

[64] A. P. Jardosh, E. M. Belding-Royer, K. C. Almeroth, and S. Suri, "Real-world environment models for mobile network evaluation," to appear in Journal on Selected Areas in Communications, special issue on Wireless Ad Hoc Networks, 2005. [Online]. Available: http://www.cs.ucsb.edu/~ebelding/courses/284/w04/papers/jardosh%5fobstacle.pdf

[65] X. Hong, M. Gerla, G. Pei, and C. Chiang, "A group mobility model for ad hoc wireless networks," in *Proceedings of ACM/IEEE MSWiM'99 – International Workshop on Modeling and Simulation of Wireless Systems*, Seattle, WA, Aug. 1999, pp. 53–60.

[66] H. Labiod, "Group mobility models for mobile ad hoc networks," in *International Conference on Advances in Infrastructure for e-Business, e-Education, e-Science, e-Medicine, and Mobile Technologies on the Internet*, L'Aquila, Italy, Jul.–Aug. 2003.

[67] V. Davies, "Evaluating mobility models within an ad hoc network," Master's thesis, Colorado School of Mines, 2000.

[68] S. Shah, E. Hernandez, and A. S. Helal, “Cad-hoc: A cad like tool for generating mobility benchmarks in ad-hoc networks,” in *Proceedings of SAINT ’02 – Symposium on Applications and the Internet*, Nara City, Japan, Jan.–Feb. 2002, pp. 270–280.

[69] T. S. Rappaport, S. S. Y., and T. K., “Statistical channel impulse response models for factory and open plan building radio communicate system design,” *IEEE Transactions on Communications*, vol. 39, no. 5, May 1991.

[70] Addition to the ns network simulator to handle Ricean and Rayleigh fading. [Online]. Available: http://www.ece.cmu.edu/wireless/

[71] M. Takai, R. Bagrodia, K. Tang, and M. Gerla, “Efficient wireless network simulations with detailed propagation models,” *Wireless Networking*, vol. 7, no. 3, pp. 297–305, 2001.

[72] M. Takai, R. Bagrodia, A. Lee, and M. Gerla, “Impact of channel models on simulation of large scale wireless networks,” in *Proceedings of ACM/IEEE MSWiM’99 – International Workshop on Modeling and Simulation of Wireless Systems*, Seattle, WA, Aug. 1999, pp. 7–14.

[73] J. Heidemann, N. Bulusu, J. Elson, C. Intanagonwiwat, K. Lan, Y. Xu, W. Ye, D. Estrin, and R. Govindan, “Effects of detail in wireless network simulation,” in *Proceedings of the SCS Multiconference on Distributed Simulation*, Phoenix, AZ, Jan. 2001, pp. 3–11.

[74] M. Takai, J. Martin, and R. Bagrodia, “Effects of wireless physical layer modeling in mobile ad hoc networks,” in *Proceedings of MobiHoc ’01 – Second ACM Symposium on Mobile Ad Hoc Networking and Computing*, Long Beach, USA, Oct. 2001, pp. 87–94.

[75] D. Cavin, Y. Sasson, and A. Schiper, “On the accuracy of MANET simulators,” in *Proceedings of the second ACM international workshop on Principles of Mobile Computing*, Toulouse, France, Oct. 2002, pp. 38–43.

[76] K. Pawlikowski, J. Jeong, and R. Lee, "On credibility of simulation studies of telecommunication networks," *IEEE Communications Magazine*, vol. 40, no. 1, pp. 132–139, Jan. 2002.